Physics – Uspekhi **61** (10) 929 – 951 (2018)

REVIEWS OF TOPICAL PROBLEMS PACS numbers: 47.27.Cn, **47.37.+q**, 67.25.dg, 67.25.dt

Acoustic turbulence of second sound waves in superfluid helium

V B Efimov

DOI: https://doi.org/10.3367/UFNe.2018.03.038317

Contents

Abstract. The anomalously strong amplitude dependence of the second sound wave velocity allows experimentally studying the behavior of nonlinear waves in a linearly dispersive medium, the processes of energy transformation from single-frequency harmonic pumping into the high-frequency dissipation edge of the spectrum, and the formation and decay dynamics of direct and inverse energy cascades.

Keywords: superfluid helium, acoustic turbulence, turbulence, second sound, nonlinear waves

1. Introduction

As is well known, motions in liquids and gases can be divided by their type into two sharply distinct classes: quiet and smooth flows, called *laminar*, characterized by predictable behavior and allowing an exact description, and their opposite, *turbulent* flows, showing disordered pulsations in the velocity, pressure, temperature, and other hydrodynamic quantities, varying unpredictably in time and space [1, 2]. Turbulence is presumably the most frequently encountered phenomenon in the Universe. It occurs in strongly nonlinear media with weak dissipation and many degrees of freedom subject to large perturbations (deviations from their equilibrium). An external action exceeding a threshold level can drive a system away from equilibrium either entirely or partly. Then either the perturbed state of the entire system or its locally perturbed state returns to its equilibrium in the presence of strong dissipation, or the perturbation propagates into the neighboring parts of the system, disturbing their equilibrium. As a result, an excitation wave propagates in the medium.

Linear motions or linear waves obey the superposition principle, according to which the propagation of waves through each other without interaction cannot create unpredictable behavior, i.e., turbulence. For wave interaction, it is required that the waves be nonlinear or, if linear, then such that they do not obey the superposition or additivity principle: two interacting linear waves with small amplitudes can create a nonlinear wave with characteristics different from those of the linear wave. Of special interest are mechanisms of energy exchange in intense nonlinear waves, in particular, the energy transfer between the pumping and dissipation intervals, influenced by wave dispersion and dissipative processes. As a simple example, we consider propagation and interaction of nonlinear waves in a medium without dispersion, or with a linear dispersion relation

$$k \sim \omega\,, \tag{1}$$

where k is the wave vector magnitude and ω the wave frequency. The propagation of a nonlinear wave with negligible dissipative processes was analyzed by Riemann [3] for an equation with the canonical form

$$u_t + uu_x = 0\,. \tag{2}$$

Here, u is a variable characterizing wave motion, typically the wave amplitude. In (2), the effect of the medium on wave

V B Efimov Institute of Solid State Physics, Russian Academy of Sciences, ul. Akademika Osip'yana 2, 142432 Chernogolovka, Moscow region, Russian Federation;
Landau Institute for Theoretical Physics, prosp. Akademika Semenova 1B, 142432 Chernogolovka, Moscow region, Russian Federation
E-mail: victor_efimov@yahoo.co.uk, efimov@issp.ac.ru

Received 18 July 2017
Uspekhi Fizicheskikh Nauk **188** (10) 1025 – 1048 (2018)
DOI: https://doi.org/10.3367/UFNr.2018.03.038317
Translated by S D Danilov; edited by A M Semikhatov

propagation, namely, the effect of viscosity and related wave absorption, is disregarded.

An equation describing nonlinear behavior in a medium with damping was first proposed by Bateman in 1915 [4]; later, Burgers proposed Eqn (3) as the simplest model of hydrodynamic turbulence [5], clarifying many aspects of model turbulence behavior in follow-up work [6, 7]. Solutions of the Burgers equation correctly describe the propagation of nonlinear waves in media with a linear dispersion relation, in particular, their steepening because of the nonlinearity and dissipation through viscosity:

$$u_t + uu_x = \nu u_{xx}\,, \tag{3}$$

where the right-hand side describes viscous dissipation.

Theoretical aspects of nonlinear processes with a detailed analysis of the Burgers equation are addressed in numerous books and articles, including those in *Physics–Uspekhi* (see, e.g., [8–17]). These studies thoroughly treat theoretical questions of nonlinear wave dynamics taking the momentum conservation and energy dissipation rate into account, as well as the evolution of unipolar pulses and random saw-tooth and periodic waves, including those in resonance conditions in an acoustic resonator. Based on the Burgers equation, a mathematical model has been proposed for the formation of the large-scale structure of the Universe [18].

Experimental realizations of wave processes obeying the Burgers equation are for the most part connected with large-amplitude nonlinear acoustic waves, whose dispersion law is close to linear. An extensive review of related works is given in Ref. [19].

Studies of nonlinear effects in sound wave propagation in air [20] and liquids [21–24] began in the middle of the 20th century. These experiments have shown that nonlinear properties of the medium play a notable role in the propagation of even moderately intense sound waves, contrary to a widespread opinion that nonlinearity is unessential for wave propagation in liquids. The formation of saw-tooth signals from a harmonic wave launched in a waveguide and the interaction of two nonlinear waves passing through each other were observed experimentally. Theoretical models were proposed and the experimental discovery was made of parametric signal amplification by two interacting acoustic waves [25–28].

An example of nonlinear waves in a medium with a linear dispersion relation is provided by second sound waves observed in experiments in superfluid helium, for which the nonlinearity coefficient is exceptionally high. This allows working with thermal waves, whose amplitude is small compared to the ambient medium temperature (small perturbations), while manifestations of nonlinear effects are seen over distances of several centimeters from the source for the Mach number $M = u/c_{20} \sim 10^{-4}$, where c_{20} is the speed of small-amplitude waves; in contrast, in air, for analogous nonlinear processes and similar Mach numbers, discontinuities in a harmonic wave with a frequency of 1 kHz form over a distance of several kilometers [29]. Furthermore, for second sound waves in superfluid helium, not only the magnitude of the nonlinearity coefficient but also the nonlinearity sign can be varied from negative to positive, which substantially broadens the possibilities of experimental research on nonlinear waves described by the Burgers equation. In particular, this allows studying the behavior of U and N waves for a thermal pulse propagating in a three-dimensional geometry in superfluid helium [30]. In a propagating bipolar wave (for example, a sound wave with regions of compression and rarefaction, or a second sound wave with regions of heating and cooling), shock waves of compression and rarefaction move apart for a positive nonlinearity coefficient. This is an example of a U wave. For a negative nonlinearity coefficient, the waves come closer and absorb one another; such waves are referred to as N waves.

In one-dimensional geometry, a propagating rectangular pulse of second sound is transformed into a triangular pulse with a discontinuity at the wave front or the trailing edge, depending on the temperature (and nonlinearity sign), and its amplitude decreases because of the nonlinearity and weak dissipation. The shape of such wave formations is described fairly well by a self-similar solution of the Burgers equation, determined by the acoustical Reynolds number $\mathrm{Re}_{\mathrm{ac}}$ [9, 17].

It is evident that as the triangular pulse propagates, its amplitude and nonlinear dependence of the velocity decrease owing to the increasing pulse duration, which reduces $\mathrm{Re}_{\mathrm{ac}}$. Additionally, the signal decays because the medium is nonideal and there is friction against the waveguide walls. We note that for second sound waves propagating in superfluid helium, we can also vary the coefficient of inviscid damping by introducing quantum vortices into the system in a controlled way. This provides one more degree of freedom for changing the conditions of acoustic wave propagation and dissipation in carrying out experiments.

In this paper, we consider experimental manifestations and theoretical results pertaining to the propagation of weakly attenuating strongly nonlinear waves of second sound in superfluid helium, a medium with a linear dispersion relation, using an example of a cylindrical resonator. Such experiments allow studying energy fluxes in acoustic turbulence and the processes of formation and decay for a direct (toward higher frequencies with respect to the driving frequency) and inverse (toward lower frequencies) energy cascades in the simplest quasi-one-dimensional geometry.

2. Nonlinear waves of second sound in superfluid helium

A peculiar feature of superfluid helium is the existence of two components, normal and superfluid, whose independent motions determine its unique properties. The ordered motion of excitations entrains only a part of the fluid, its normal component with a density ρ_{n}. The remaining part, the 'superfluid' component with the density $\rho_{\mathrm{s}} = \rho - \rho_{\mathrm{n}}$, performs independent potential motion. The presence of two independent components of fluid motion gives rise to several forms of weakly attenuating oscillations, including the first and second sounds. For sound waves of density or pressure (the first sound), the solutions are found from [1]

$$\frac{\partial^2 \rho}{\partial t^2} = \Delta p\,, \tag{4}$$

where p is the pressure. Equations of two-fluid hydrodynamics contain one more solution: the waves of second sound (thermal waves or entropy waves)

$$\frac{\partial^2 \sigma}{\partial t^2} = \frac{\rho_{\mathrm{s}}}{\rho_{\mathrm{n}}}\,\sigma^2 \Delta T\,, \tag{5}$$

[1] We skip the details of the two-component fluid dynamics of superfluid helium, which are thoroughly described, for example, in Ref. [31].

where σ is the entropy density. The second sound wave can be described as a density wave in a gas of excitations for which the pressure and density in real space do not change,

$$\rho = \rho_n + \rho_s = \text{const} \quad \text{or} \quad \frac{\partial \rho_n}{\partial t} = -\frac{\partial \rho_s}{\partial t}\,, \tag{6}$$

$$j' = \rho_n v'_n + \rho_s v'_s = 0\,, \tag{7}$$

where v'_n and v'_s are velocity (or flux) variations of the normal (n) and superfluid (s) components. In a second sound wave, the normal and superfluid components move in opposite directions, such that the total mass transport remains unchanged.

For waves with small amplitudes ($\Delta T/T \ll 1$ and $\Delta p/p \ll 1$), because of the smallness of the thermal expansion coefficient in helium-II [$(\partial\rho/\partial T)_p \ll 1$, which leads to approximately equal specific heats $C_p \approx C_V$], two waves (of density and temperature, the waves of the first and second sounds) can propagate with the speeds given by

$$c_1 = \sqrt{\frac{\partial p}{\partial \rho}}\,, \tag{8}$$

$$c_2 = \sqrt{\frac{\rho_s \sigma^2}{\rho_n}\frac{\partial T}{\partial \sigma}}\,. \tag{9}$$

A theoretical approach to detecting second sound was proposed by Lifshitz [32]. It was discovered experimentally by Peshkov [33, 34].

Taking the finite coefficient of thermal expansion in liquid helium into account gives rise to a coupling between the first and second sound waves, which increases in approaching the superfluid transition temperature. For example, the coefficient of thermal expansion is 2×10^{-4} K^{-1} at the temperature $T = 1.2$ K, 2.5×10^{-3} K^{-1} at $T = 1.5$ K, 1×10^{-2} K^{-1} at $T = 1.9$ K, and $\sim 2 \times 10^{-1}$ K^{-1} at $T = 2.08$ K, where most measurements were carried out [35]. The weak dependence of density on temperature is the basis for the measurements of the first sound amplitude carried out in Ref. [36] using a superconducting bolometer.

The propagation of thermal waves in superfluid helium, in contrast to such waves in most of other substances, is due to their wave nature, and not the diffusive heat propagation whereby the wave decays at distances comparable to the wavelength. The attenuation of second sound waves is remarkably weak, which is due to the two-fluid nature of thermal waves in superfluid helium. At low frequencies (less than 100 Hz), the attenuation of second sound waves propagating in helium is determined not by the bulk viscosity but mainly by wave-induced friction against the waveguide walls.

For any turbulent process, its dissipation is determined by viscous processes. In this respect, it is of interest to compare the kinematic viscosity coefficients ν for various media.

From the table below, an unambiguous conclusion can be drawn about the unique properties of helium (especially in the superfluid phase), which allow a reduction in the size of experimental setups intended for studies of turbulence in various manifestations owing to its exclusively small viscosity [37–40]. The governing principles in this case are those of similarity based on the characteristic geometric size of the system L and a characteristic velocity V (the Reynolds number $\mathrm{Re} = VL/\nu$); accounting for external forces, for example, gravity, introduces one more dimensionless parameter: the Froude number, as well as the Prandtl number when accounting for thermal conductivity, and so on. For us, of importance here are the dimensionless parameters for acoustic wave processes [41], in which considerable changes in hydrodynamic wave parameters occur on a characteristic length scale, dominated by nonlinear (Z_{NL}) or dissipative (Z_{dis}) processes,

Table. Kinematic viscosity coefficients for some substances.

Medium	Temperature, K	ν, cm^2 s^{-1}
Glycerine	293.15	6.8
Air	293.15	0.15
Alcohol	293.15	0.022
Water	293.15	0.010
Mercury	293.15	1.2×10^{-3}
Helium (gas)	5.5 (for $p = 2.8$ bar)	3.21×10^{-4}
Liquid helium	2.25 (at SVP)*	1.96×10^{-4}
Superfluid helium	1.8 (at SVP)*	9.01×10^{-5}
* SVP: saturated vapor pressure.		

$$\frac{Z_{\mathrm{NL}}}{Z_{\mathrm{dis}}} \sim \frac{\rho V L}{\eta} = \frac{V\lambda}{\nu} = \mathrm{Re}_{\mathrm{ac}}\,, \tag{10}$$

where a change in the oscillatory or acoustic velocity occurs at a wavelength λ, the characteristic time scale in this case being $\sim 1/\omega$ ($\eta = \nu\rho$ is the dynamic viscosity). An essential parameter describing nonlinear effects is the Mach number, reflecting the influence of nonlinear effects on wave propagation:

$$M = \frac{u}{c_{20}}\,. \tag{11}$$

Although nonlinear effects have been observed in various gases and liquids, it is very likely that most rigorous and unambiguous results can be obtained with second sound waves because of their special properties, which give them an advantage over nonlinear waves in other media.

A characteristic feature of second sound waves in superfluid helium is the absence of dispersion, i.e., the absence of the dependence of the wave speed on frequency in the experimental frequency range (up to several mHz) [42]. The second sound frequency depends on the wave vector as [43]

$$\omega = c_{20} k \left(1 + \lambda_0 \xi^2(T) k^2 + \ldots\right), \tag{12}$$

where $\xi(T) = \xi_0 (1 - T/T_\lambda)^{-2/3}$, $\xi_0 \sim 2-3$ Å, and $\lambda_0 \sim 1$. We stress that the dispersion of second sound becomes noticeable only in a close vicinity of the superfluid transition (i.e., for $T_\lambda - T < 1$ μK) and is negligibly small for temperatures $T < 2.1$ K. This allows considering the interaction of collinear waves as three- and four-wave processes with energy and momentum exchanges.

For temperatures $T > 0.9$ K (roton second sound) and at frequencies below the phonon–roton (ph–r) interaction [44],

$$\omega < \frac{c_{20}}{c_{10}} \frac{1}{\tau_{\mathrm{ph-r}}}\,, \tag{13}$$

where c_{10} and c_{20} are the speeds of the first and second sound waves of infinitesimal amplitude, the spectrum $\omega(k)$ is a linear function of the wave vector k defined by (1) [31]. The condition $\omega\tau_{\mathrm{ph-r}} \sim c_{20}/c_{10}$ can be written as $l_{\mathrm{ph}} \sim \lambda$, where l_{ph} is the photon mean free path and λ is the wavelength of the second sound. Thus, dispersion for second sound is observed at such frequencies where the second sound wavelength becomes comparable to the phonon mean free path. Experimental searches for second sound dispersion have been carried out by Peshkov [45], and no deviation from linearity in the frequency range from 10 Hz to 10 kHz was found.

The dispersionless nature of thermal waves allows the second sound in superfluid helium to be used as an object to study wave interaction in the one-dimensional (quasi-one-dimensional) geometry, the simplest one from the standpoint of the mathematical description. In this geometry, waves are collinear, their behavior and interaction are governed by their nonlinear properties, and both three-wave and four-wave interactions are possible, including three-wave processes of wave merger and decay:

$$\omega_1 + \omega_2 \to \omega_3\,, \qquad k_1 + k_2 \to k_3\,, \tag{14}$$

$$\omega_1 \to \omega_2 + \omega_3\,, \qquad k_1 \to k_2 + k_3\,. \tag{15}$$

A nonlinear wave is characterized by the dependence of its speed on its amplitude. In the simplest case, we can express the dependence of the wave speed c on its amplitude A as

$$c = c_0(1 + \alpha A)\,, \tag{16}$$

where c_0 is the wave speed of an infinitesimal wave, α is the wave nonlinearity coefficient, and A is the amplitude, which can be identified with the wave height H for a surface wave in fluids, Δp for pressure waves, $\Delta\rho$ for density waves, ΔT for thermal waves, and so on. In this respect, the second sound waves in superfluid helium offer experimenters a unique possibility: the speed of these waves shows a strong dependence on both their amplitude and the temperature at which the experiments are carried out. The nonlinearity coefficient can attain large positive values, stay equal to zero, and even become negative (Fig. 1), which is not observed for almost any other acoustic waves. Furthermore, as the temperature approaches the lambda point T_λ, the negative nonlinearity coefficient tends to infinity, and the speed of second sound waves tends to zero. The existence of an anomalously large nonlinearity coefficient in superfluid helium has the consequence that the propagation of second sound (thermal) waves with even a rather small amplitude ($\delta T/T \ll 1$) is accompanied by the occurrence of discontinuities either at the front or the trailing slope (depending on the nonlinearity sign) over a path of several centimeters. In the same way, a harmonic wave is enriched with multiple harmonics for a fairly small system size.

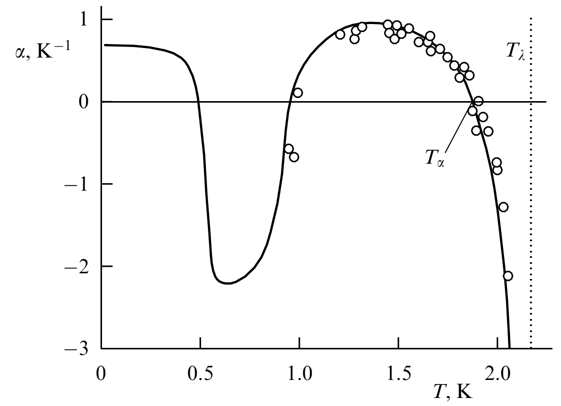

Figure 1. Dependence of the nonlinearity coefficient for the second sound velocity on temperature. The solid curve presents Khalatnikov's computations [46], the circles are experimental results from Ref. [47].

Computations performed in [46] express the nonlinearity coefficient for second sound as

$$\alpha_2(T) = \frac{\sigma T}{C}\frac{\partial}{\partial T}\ln\left(c_{20}^3\,\frac{C}{T}\right). \tag{17}$$

The theoretical curve and measurement results are given in Fig. 1.

We used these unique properties of helium to model and experimentally study the propagation of strongly nonlinear waves in a medium characterized by a linear dispersion relation and weak attenuation.

A fundamental advantage of working with nonlinear second sound (thermal) waves is that their amplitude is a small perturbation of the ambient temperature, whereas, for example, in sound waves in conventional media, the pressure perturbation p' is not necessarily small. The velocity amplitude u in nonlinear acoustic waves (2) is defined as

$$u = \frac{p'}{\rho c_0}\,. \tag{18}$$

In air, the nonlinearity coefficient α in formula (16) is ≈ 1.2, while $\alpha \approx 4$ in water, which, it may seem, should imply that the effect of nonlinearity on wave propagation processes is significant. A nonlinear acoustic wave (for example, in water) propagates with the speed

$$c = c_0 + \alpha u = c_0\left(1 + \frac{\alpha u}{c_0}\right) = c_0\left(1 + \frac{\alpha}{c_0}\,\frac{p'}{\rho c_0}\right). \tag{19}$$

If a sound wave pressure $p' \sim 1$ atm is inserted in (19), as defined by limitations imposed on the wave amplitudes by possible cavitation at small depths, we find the Mach number $M = \Delta c/c_0$ of the order of 10^{-4}; in contrast, for second sound waves such Mach numbers can be obtained for thermal waves with the amplitude $\delta T \sim 10^{-4}$ K, which is small compared to the temperature of the fluid $T \approx 2$ K.

In superfluid helium with propagating second sound waves, the simplest situation can be realized, that of one-dimensional (or quasi-one-dimensional in experiments) interacting nonlinear waves in a medium with a linear dispersion relation. In experiments, we studied propagation and multiple self-intersections of a wave that was initially harmonic at its pumping frequency and was strongly distorted due to nonlinearity.

Acoustic turbulence, according to the definition formulated by Zakharov and Sagdeev [48], is the turbulence of compressible fluid such that the fluid motion is potential, representing an ensemble of interacting sound waves. If wave dispersion is weak or fully absent, the properties of turbulence are determined by strong interaction among a large number of coherent wave harmonics.

In describing acoustic turbulence governed by nonlinear interaction among many waves (or multiple harmonics), we have to take into account not only the nonlinear transformation of these waves but also kinetic relations of three- and four-wave processes for multiple harmonics initiated by a pumping wave. (For more details on the analysis of nonlinear acoustic equations, see monograph [17].)

In carrying out experiments in superfluid helium, the existence of quantum vortices must be taken into account. In superfluid liquids, in addition to classical vortex motion, which decays with time due to viscous losses, quantum nondecaying vortical motion of the superfluid component — quantum vortices — can be present. The motion of a body with high velocities in superfluid helium would result in a turbulent state, quantum turbulence, whose behavior is also governed by quantum properties of He-II, especially at temperatures $T \to 0$ [49]. Counterflows of the normal and superfluid components due to propagating second sound waves also lead to increasing the vortex system density. However, this increase is observed for heat fluxes in excess of 30–50 mW cm^{-2} [50, 51], limiting the excitation level of second sound waves in our experiments.

The idea of using second sound to study the behavior of nonlinear waves was first discussed by Khalatnikov [31]. Indeed, superfluid helium, given its properties, is an ideal model system to explore nonlinear waves and Burgers turbulence. Using the Burgers equation to describe nonlinear finite-amplitude waves in superfluid helium was proposed in [52, 53]. However, experimental research has demonstrated that the propagation of such waves in real situations is more complicated than predicted by a simple theoretical analysis of the Burgers equation and Burgers turbulence.

3. Experimental technique

The complexity of experiments with second sound waves in superfluid helium is related to the low temperatures needed to carry out the experiments, requirements regarding careful work with a moderate vacuum, and measurement peculiarities of small-amplitude thermal waves. Experimental temperatures for superfluid transition (below $T_\lambda \approx 2.17$ K) are achieved in our experiments by pumping out helium-4 vapor.

In experimental studies of second sound waves, we followed a technique traditionally used for already more than 60 years, beginning from the time second sound waves were discovered: the excitation of standing waves in a cylindrical resonator, with a plane heater fitted to one of its ends and a thermometer to the other. The advantage of this setup is that to excite a periodic wave with a relatively high amplitude, it suffices to apply a weak exciting harmonic signal to the heater at the resonance frequency. Weak harmonic heating creates only a relatively weak stationary heat flux; large stationary heat fluxes could trigger the development of a vortex component.

Judging by the method of generation and registration of second sound waves, all experimental techniques can be divided into two groups. In the techniques belonging to the first group, the sensitive elements are thermometers of different types, showing high sensitivity at low temperatures, for example, superconducting or semiconducting films [33, 52, 54–60] and film heaters. Techniques of the second kind for detecting waves in superfluid helium are based on the ability of the superfluid component to penetrate through small pores in membranes, which are impermeable to the flow of the normal component [61–63]. The superfluid component filling a closed volume changes the pressure there and bends the membrane, which is recorded as a change in capacitance of a capacitor having the membrane as one of its plates. A generator of second sound can work by the same principle, creating a varying flow of the superfluid component.

In experiments, we used the superconducting properties of thin tin–copper films deposited on a quartz or glass substrate. The sensitivity of bolometers manufactured with this technology reached the level of ~ 10 V K^{-1}, which allowed the detection of thermal waves with an amplitude of several μK and temporal resolution better than $\tau < 0.1$ μs, which corresponds to frequencies up to $f \sim 10$ MHz. The minimum second sound wavelengths with which it was possible to work using superconductive bolometers are ~ 2 μm.

Film heaters were used in experiments as a source of second sound. The threshold stationary heat fluxes at which the density of the vortex system starts to increase are $\sim 30-50$ mW cm^{-2} [50, 51, 64, 65]. In our experiments, we worked with powers smaller than these, and therefore the changes in the vortex system could be ignored when considering the dynamics of turbulent processes in second sound waves.

Eigenfrequencies of the resonator. For most of the experiments described below, we used a cylindrical resonator with the inner diameter $D = 16$ mm and length $L = 70$ mm. To test the effects observed, resonators of other sizes were used, for example, with the length $L = 20$ mm. The film heater had a meandering shape to create uniform heating over the entire section of the cylinder and occupied the entire cylinder cross section. The eigenmodes of oscillations in a cylindrical resonator can be defined as [66]

$$f_{pmn} = \frac{1}{2} c_{20} \left[\left(\frac{p}{L} \right)^2 + \left(\frac{2a_{mn}}{D} \right)^2 \right]^{1/2}, \tag{20}$$

where the integers p, m, and n are the mode numbers for the harmonics of the resonator. The quantity a_{mn} is a solution of the equation

$$\frac{\mathrm{d}J_m(\pi a)}{\mathrm{d}a} = 0\,, \tag{21}$$

where $J_m(\pi a)$ is the Bessel function of the mth order.

In the case of a cylindrical resonator, despite precautions taken to ensure uniform heating, radial ('Bessel') modes were excited, in addition to longitudinal oscillations. The generation of radial modes by longitudinal modes from the heater can be explained, among other factors, by the not truly uniform profile of the counterflows of the superfluid and normal components because of the friction of the latter against the resonator walls. As a result, if the frequency of such a wave fits in a radial resonance, the generation of radial modes can be observed. The excitation of Bessel modes by a flat 'uniform' heater in a cylindrical resonator was observed previously in Refs [34, 54, 67].

Plane waves in the resonator correspond to solutions with $a_{00} = 0$, and frequencies for such resonances are expressed as $f_p = (1/2)c_2 p/L$. In our experiments, we also observed radial modes with nonzero n. For a resonator with $L = 70$ mm and $D = 16$ mm, the first radial mode was very close to the 11th longitudinal resonance.

Resonator Q factor. The Q factor of the resonator is of fundamental importance in experiments with nonlinear standing waves of second sound. Most attention in the fabrication of the resonator was paid to keeping its ends parallel to each other and perpendicular to the cylinder axis. The Q factor of the resonator measured in our experiments was about several thousand for resonances with numbers $N > 10$. For resonances with the smallest numbers, the Q factor was lower. At low frequencies ($f < 10$ kHz), the resonator Q factor can be expressed as

$$Q \sim \frac{1}{L_{\mathrm{N}}\Lambda} \sim \omega^{3/2}\,, \tag{22}$$

where $\Lambda \sim 1/\sqrt{\omega}$ is the penetration depth of viscous wall friction and L_{N} is the distance the wave propagates before it loses phase because of the nonparallel ends of the resonator cylinder (ΔL), which reflect second sound waves (in our case, $\Delta L/L \sim 5\times10^{-4}$). We note that the wavelength λ becomes smaller than ΔL at frequencies higher than 100 kHz.

For the resonance frequency ~ 1000 Hz, the penetration depth of viscous friction is of the order of 2.5 μm ($T = 2.08$ K). The Q factor can then be determined as the ratio of the area of the freely moving fluid to the area of fluid delayed by friction at the distance Λ from the walls, $(\pi D^2/4)/(\pi D\Lambda) \sim 1000$, which is close to the values observed experimentally. Thus, the Q factor of the resonator of second sound waves at low frequencies is mainly determined by surface losses, which, as mentioned in Ref. [67], is explained by the dominance of surface damping over the bulk damping for second sound at temperatures above 1.3 K.

At high frequencies (for resonances with large numbers), the Q factor is determined by second sound bulk damping, $\nu \sim \omega^2$, which prevails at frequencies higher than 100 kHz.

For acoustic turbulence, the development of turbulent processes is governed by the acoustic Reynolds number $\mathrm{Re}_{\mathrm{ac}}$, which reflects the relation between nonlinear processes causing distortion of the wave profile and the processes of wave dissipation in the course of propagation [see Eqn (10)]. For second sound waves in superfluid helium, the Reynolds number in the resonator is expressed as [68, 69]

$$\mathrm{Re}_{\mathrm{ac}} = \frac{\alpha_2 u_{20}}{\gamma}\left(\frac{\partial\delta T}{\partial x}\right) \sim \alpha_2 Q\delta T\,. \tag{23}$$

Propagation of nonlinear waves in the resonator is accompanied by interaction among all harmonics and modes. This interaction becomes especially strong if resonance occurs at multiple frequencies, when excitation of harmonic oscillations in a closed resonator produces a standing wave. In this case, the wave field can be represented as a superposition of two waves traveling in opposite directions [70–74]. For plane density waves in a viscous heat-conducting fluid in the first approximation (ignoring nonlinearity and attenuation), the solution is given by arbitrary perturbations propagating in the positive and negative directions of the x axis and preserving their shape. Resonant oscillations in a resonator with a linear dispersion relation and weak attenuation are governed by the parameter $\Sigma = [\alpha u_0\omega/(2c_0)]t$ characterizing the degree of manifestation of nonlinearity, with the nonlinearity coefficient α, and for $\Sigma = 1$ the profile of each of the counter-propagating waves becomes multivalued, which corresponds to the discontinuity formation. The time it takes for the discontinuity (a shock) to develop in the initially harmonic wave is [75]

$$t_{\mathrm{br}} = \frac{T}{\pi M}\,, \tag{24}$$

where T is the period of oscillations and $M = \Delta c/c_0$ the Mach number.

We note that for waves propagating in the resonator in the positive-x direction, the solution is described by the Burgers equation.

Qualitatively, the behavior of resonant oscillations of a harmonic wave in a waveguide with damping can be seen as passing through three temporal stages. The first stage lasts from the initial moment until t_{br} when nonlinear distortions of a harmonic large-amplitude wave are accumulated and energy starts being transferred to higher frequencies, but dissipation can still be disregarded. The second stage begins when shock fronts in traveling waves have already formed, accompanied by energy absorption at higher frequencies. Finally, in the third stage, the energy transfer to higher frequencies has already ceased, the energy injected into the system initially is strongly reduced via dissipative processes, and only propagating sinusoidal waves of small amplitude are left. On a qualitative level, similar stages can be partly observed as a standing wave is formed in a resonator and decays when pumping is switched off. The solution for forced nonlinear waves in a resonator with damping, proposed in [74], approximately corresponds to the arrangement of our experiments, in which, in particular, we estimated the effect of the acoustic Reynolds number on the resonator Q factor.

The resonator Q factor has two parts: linear and nonlinear. The ratio of 'amplitudes' of a standing nonlinear wave and boundary oscillations grows with time and reaches a stationary limit having the meaning of a stationary nonlinear Q factor,

$$Q_{\mathrm{NL}} = \sqrt{\frac{c}{2\alpha A}}\,. \tag{25}$$

For small nonlinearity, the resonator Q factor is independent of the amplitude of oscillations and is determined by the usual linear absorption,

$$Q_{\mathrm{L}} = \frac{1}{2D} = \frac{c^3\rho}{b\omega^2 L} = \frac{c^2\rho}{\pi b\omega}\,, \tag{26}$$

where b is the effective medium viscosity.

To compare the results of measurements, we consider several particular solutions of the general inhomogeneous equation describing oscillations forced with a harmonic external force:

$$u(x=0,t) = -\frac{M}{2}\sin\xi\,, \qquad u(x=L,t) = 0\,, \tag{27}$$

where $\xi = \omega t + \pi$ and $M = A/c_0$ are dimensionless variables and A is a characteristic amplitude.

Leaving aside the details of mathematical substitutions and transformations, we only write the equation describing each of the counter-propagating nonlinear waves [75, 76]:

$$\frac{\partial U}{\partial T} + \Delta\frac{\partial U}{\partial\xi} - \pi\alpha U\frac{\partial U}{\partial\xi} - D\frac{\partial^2 U}{\partial\xi^2} = -\frac{M}{2}\sin\xi\,. \tag{28}$$

Here, U is an arbitrary function describing the profile of nonlinear traveling waves, normalized with the wave speed c, $T = \omega t/\pi$ is the dimensionless time variable, Δ is the frequency detuning (the difference between the given and resonance frequencies), and $D = b\omega^2 L/(2c^3\rho)$ is the dimensionless dissipative parameter, $D \ll 1$ for weak dissipation.

If the frequency detuning is zero ($\Delta = 0$, resonance conditions), the solution can be expressed as a series in even Mathieu functions [17]; for zero initial conditions, $U(T=0,\xi) = 0$, the function U begins to grow as $\sim t$. The equilibrium value of U attained at an infinite time, $t \to \infty$, under the dominant influence of nonlinear processes ($\chi = \pi\alpha M/(2D^2) \gg 1$, where χ is the ratio of nonlinear coefficient to the dissipative ones) is fully independent of the linear Q factor of the system [77], being determined by the processes transferring energy from the pumping range of the nonlinear resonant system to its dissipation range. Nonlinear distortion of a harmonic wave and transformation of the frequency spectrum of interacting counter-propagating waves lead to the formation of energy fluxes to higher frequencies, where they are dissipated (the direct energy cascade).

When studying energy transfer, i.e., energy fluxes in the frequency domain from the pumping range to the dissipative edge of the spectrum, we relied on the frequency Fourier analysis of the form of recorded signals and on changes of such spectra with time.

4. Direct energy cascade in acoustic turbulence

To study a complex phenomenon such as turbulence, the most productive approach is to simplify the system so as to understand its behavior and the laws of energy transfer from the pumping range to the range of viscous dissipation under a controlled change in parameters. As such a model system, one can use a system of surface waves in waveguides of various shapes with the length reaching several hundred meters [78], and resonators of various sizes (from several centimeters to 10 m) and shapes [79, 80]. The fluid in such a model system can be water [81–83], mercury [84], or cryogenic liquids: liquid hydrogen [85] or helium [86]. In this case, gravity and capillary waves have dispersion dependences of different characters (for water, the capillary waves are replaced by surface gravity waves for wavelengths longer than $\lambda \sim 2$ mm).

We note that turbulent phenomena for waves on a fluid surface can also be attributed to acoustic turbulence, where the formation of the high-frequency spectrum is determined by competition between nonlinear and dissipative processes. The analogy becomes more transparent for quasi-one-dimensional standing or traveling surface waves in long waveguides or resonators. We now consider the subject of this paper, the nonlinear processes accompanying the propagation of second sound waves and energy transfer over the frequency range.

As shown experimentally [87], intense pulses of second sound in superfluid helium transform into shock waves practically instantaneously, forming discontinuities at wave fronts or rear slopes, depending on the sign of the nonlinearity coefficient. As T_λ is approached, the nonlinearity coefficient increases without a bound, tending to $-\infty$ for T_λ, and hence the nonlinearity plays a decisive role even for waves of a very small amplitude [88, 89].

The speed of a second sound wave $c_2 \sim 20$ m s^{-1} at $T \sim 2$ K is one to two orders of magnitude smaller than the typical speed of the first (conventional) sound in gases and condensed media. The low sound wave speed allows achieving an improved temporal resolution when measuring the profile of a sound wave compared to the case of traditional research dealing with nonlinear effects in sound waves.

The condition that thermal waves are reflected back by the ends of a cylindrical resonator implies the absence of a normal flux of the normal and superfluid components through the reflecting surfaces,

$$j = 0 \quad \text{for} \quad x = 0 \quad \text{and} \quad x = L\,. \tag{29}$$

In reality, condition (29) does not hold strictly: the heater at $x = 0$ permanently pumps energy into the system, and hence small fluxes, both constant and variable, pass through this end, just as heat and wave leak through the other end; however, in the first approximation for an experimental explanation of the effects observed, these losses can be ignored. We note that the thermal wave is excited at twice the pumping frequency, which allows the useful signal to be separated from the signal related to the electric induction at the pumping frequency.

Under the resonance condition $f_{\mathrm{d}} = c_2/(2L)$, the wave amplitude significantly increases, in agreement with the system Q factor, until the moment when the incoming energy is equilibrated by wave losses in the resonator. In this case, for sufficiently small energy pumping and small heat fluxes from the heater into the resonator volume, the wave begins to strongly amplify, whereas its shape is distorted by nonlinear processes. The magnitude of distortions depends on the pumping amplitude U_{G}, which is in fact confirmed by observations. If U_{G} is increased, the wave temperature, recorded by a bolometer, increases quadratically with the signal from the generator,

$$A \sim \delta T \sim q \sim U_{\mathrm{G}}^2\,. \tag{30}$$

For a small thermal wave pumping voltage, the losses have a linear character, being determined by the Q factor at a given frequency. The deviation from linearity [the quadratic dependence $\delta T(U_{\mathrm{G}})$] begins at the heat flux density $q > 6$ mW cm^{-2}, which is clearly seen in Fig. 2b.

For small pumping amplitudes and hence second sound amplitudes, the nonlinear effects are weak and wave distortions are not apparent, which is expressed in the absence of multiple harmonics. The increase in the wave amplitude causes wave distortion and the generation of higher harmonics. The energy flux generating this energy cascade determines the deviation from linearity (Fig. 2b). This is seen as a cascade of multiple harmonics (Fig. 3).

One possible explanation of the distortion of the second sound wave shape and hence the formation of higher harmonics is the interaction of counterflows of normal and superfluid components with vortices in helium. As is well known, heat fluxes increase the concentration of vortices in

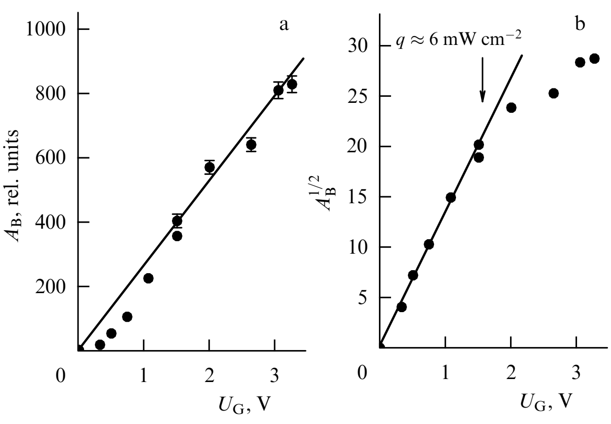

Figure 2. (a) Dependence of thermal wave amplitude A_{B} in the resonator on the pumping amplitude U_{G}. (b) Dependence of $A_{\mathrm{B}}^{1/2}$ on U_{G} (dots). The straight line in (b) corresponds to the linear dependence of the recorded signal on $q(U_{\mathrm{G}})$ [see relation (30)]. The arrow in panel (b) marks the heat flux density where the actual dependence begins to deviate from linearity. $T = 1.767$ K, the 11th resonance, $f_{\mathrm{d}} \sim 1478$ Hz, the nonlinearity coefficient is positive.

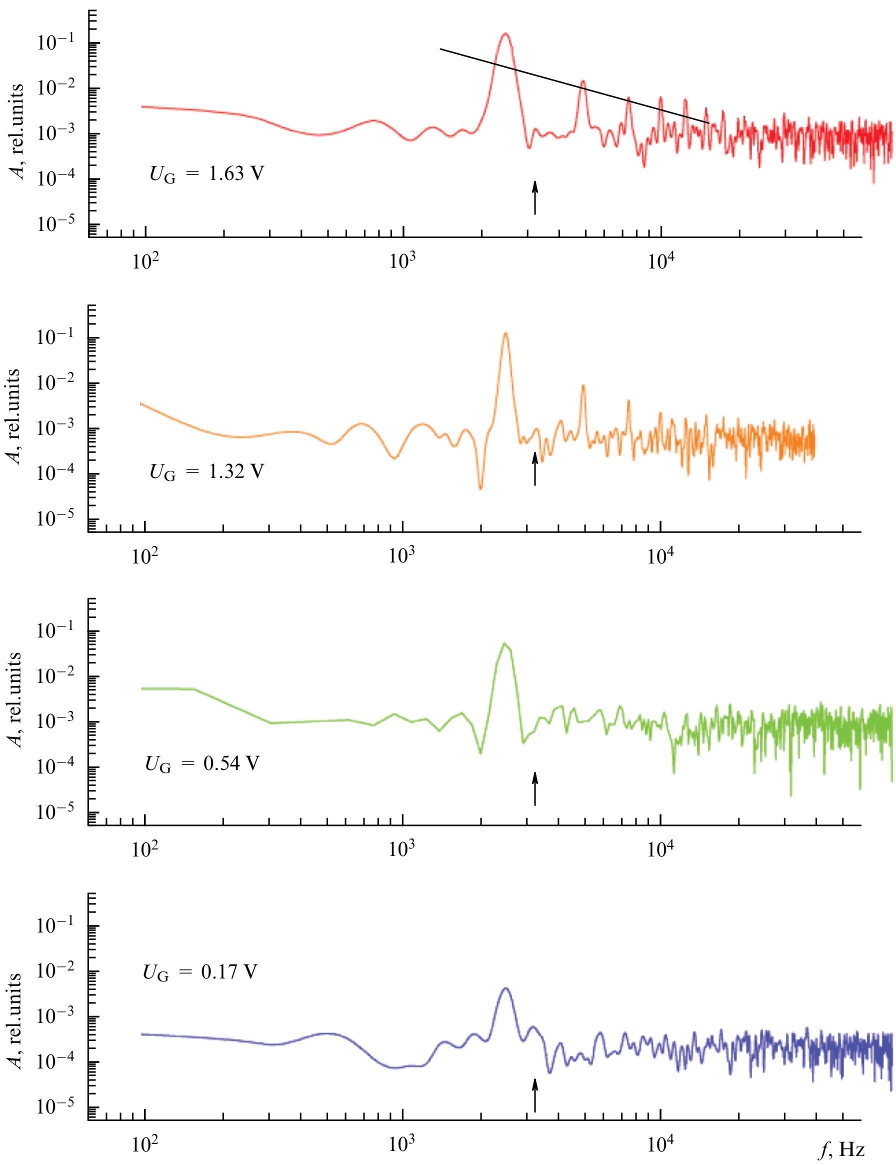

Figure 3. Formation of an energy cascade as the signal on the heater is increased, from the Fourier analysis of data in Fig. 2.

superfluid helium [64, 65, 90]; however, this phenomenon becomes noticeable for heat fluxes in excess of 30–50 mW cm^{-2}, the reason why we tried to avoid large fluxes in experiments. Remarkable properties of the second sound nonlinearity coefficient allow checking whether the observed effect of higher harmonic formation is indeed related to the nonlinear wave behavior. As the temperature approaches T_α, the nonlinearity coefficient approaches zero, and the amplitudes of higher harmonics begin to decrease. At T_α, only the main harmonic remains, and its multiple harmonics occur only for $T \neq T_\alpha$. Such a temperature dependence of the frequency spectra points at the decisive role of wave nonlinearity in the formation of harmonics. We note that at T_α, we can test the generation of nonlinear waves and discontinuities for a cubic nonlinearity, for example, when a bipolar wave with the crest temperature higher than T_α and the trough temperature lower than T_α has different values of the nonlinearity coefficient, with $\alpha_2 < 0$ and $\alpha_2 > 0$ [57].

Kolmogorov cascades. The increase in amplitude strengthens the influence of nonlinear interactions, which is manifested in higher probabilities of three-wave processes (14), leading to the formation of higher harmonics.

The shape distortion of a harmonic wave increases together with the pumping signal [90]. In the frequency domain, this is reflected in the development of a dense 'comb' of higher harmonics (the direct energy cascade) [92]. In experiments, it was possible to observe 30–50 spectral peaks with amplitudes above the noise level of the instruments, which enabled a rather reliable analysis of how their amplitudes and energies are distributed over frequency. A stationary process of energy transfer in the frequency domain occupies the range from the pumping frequency to the spectral end at high frequencies, where dissipative processes begin to dominate.

Thus, acoustic turbulence represents competition between two mechanisms changing the wave shape: nonlinear propagation, tending to form a shock wave, and dissipation, smoothing any steepening in the wave profile. Frequencies where viscous losses begin to prevail are denoted as f_b, identifying the end of the frequency range where inertial energy transfer among multiple harmonics is superseded by a process in which a high-frequency wave loses more energy through damping than it gains via energy transfer between neighboring modes.

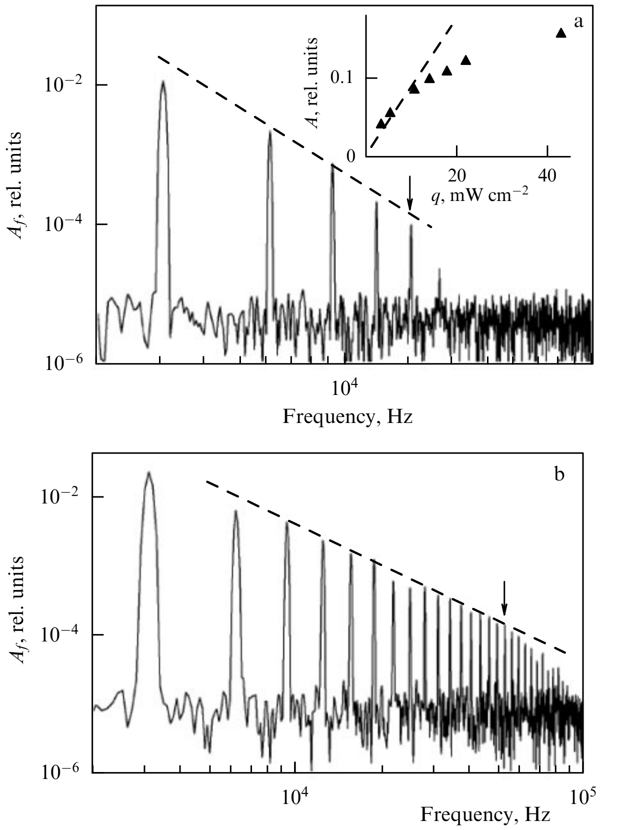

Figure 4. Amplitude A_f of standing second sound waves in a resonator for the heat flux density (a) $q = 5.5$ mW cm^{-2} and (b) $q = 22$ mW cm^{-2}. The dashed line corresponds to the dependence $A_f \sim f^{-1.5}$. The arrows mark the viscous boundary of the inertial range. The inset in panel (a) shows the amplitude of the second sound wave as a function of the heater power. The dashed line in the inset corresponds to $A \sim q$ for small pumping amplitudes. $T = 2.079$ K, the 31st resonance, the frequency $f_d = 3093.2$ Hz.

The role of three-wave processes becomes apparent if we consider the influence of the pumping amplitude on the inertial range width. For nonlinear waves, the energy transfer to multiple harmonics in three-wave interactions is governed by amplitudes of both interacting waves, and the inertial range broadens as the pumping amplitude is increased.

Figure 4 demonstrates the shift in the end of the inertial range caused by the increased signal on the heater. In the inertial range, the exponent of the power-law dependence $A(f) \sim f^{-m}$ (or $E(f) \sim f^{-2m}$ for energy) drops to 1.5.

A theoretical model of the spectral energy transfer in three-wave interactions was built in Ref. [93]. To understand how the direct energy cascade is formed, we proposed a model for the interaction of nonlinear waves, with the presence of a counterflow of normal and superfluid components in superfluid helium taken into account. Previously, such an approach to numerical modeling was used in Ref. [94]. In the framework of this model, numerical simulations were carried out with Hamiltonian variables representing second sound [95], and direct integration of wave shape modification in the resonator was performed with quadratic terms taken into account [96]. In this model, it is assumed that bulk attenuation is essential in the entire frequency range.

This model differs to some degree from the experimental situation in real resonators (where bulk attenuation supersedes the surface one and becomes dominant only for harmonics with numbers $N > 100$) but, in general, appropriately describes the results obtained in measurements.

The equation describing energy balance in a system of multiple harmonics can be written as

$$\mathrm{i}\,\frac{\partial b_n}{\partial t} = \sum_{n_1, n_2} V_{n, n_1, n_2} \left(b_{n_1} b_{n_2} \delta_{n-n_1-n_2} + 2 b_{n_1} b^*_{n_2} \delta_{n_1-n_2-n} \right) - \mathrm{i}\gamma_n b_n + F_{\mathrm{d}n}\,, \qquad (31)$$

where b (with various indices) are the amplitudes of the respective harmonics, V_{n,n_1,n_2} is the probability of interaction between waves n, n_1, and n_2, $\delta_{n_1-n_2-n}$ is the delta functions defining the frequencies of two waves merging into one and one wave decaying into two, the asterisk denotes complex conjugation, γ_n is the wave attenuation coefficient, and $F_{\mathrm{d}n}$ is the external pumping at the frequency of wave n. The time evolution of the amplitude of the nth harmonics is determined by the probability of two wave harmonics n_1 and n_2 merging [the first term in parentheses in the right-hand side of Eqn (31)] and the probability that this wave decays into two waves with lower frequencies (the second term in the parentheses). The probability of wave interaction V_{n,n_1,n_2} depends on the nonlinearity coefficient α [96],

$$V_{n, n_1, n_2} = \alpha \,\mathrm{const}\,(T) \sqrt{n n_1 n_2}\,. \qquad (32)$$

Numerical integration of Eqn (31) for the standing-wave energy balance in the resonator was carried out in the case of generation at the resonance frequency. We computed the changes in the energy of each harmonic,

$$P(n) = \left\langle \left| b_n(t) \right|^2 \right\rangle, \qquad (33)$$

and the energy distribution over harmonics for a constant energy flux and a stationary spectrum:

$$E(\omega) = \omega_n P(n)\,. \qquad (34)$$

The resulting stationary distributions for the energies of harmonics for various pumping intensities in the resonator are presented in Fig. 5.

Formation of energy spectra in acoustic turbulence of second sound waves was found in both experiments and numerical simulations.

According to the main ideas in Refs [48, 97–100], such a highly excited state of a system with a large number of degrees of freedom is defined as a turbulent one. The formation of the observed direct cascade qualitatively resembles the occurrence of the Kolmogorov velocity distribution in the frequency domain in compressible fluid turbulence or in a system of capillary or gravity waves on a fluid surface [101, 102]. A distribution resembling the Kolmogorov one can be constructed for the dependence of amplitudes of multiple frequency harmonics on the developed acoustic turbulence, $A(f) \sim f^{-m}$, where $m \sim 1.5$.

As the pumping amplitude is increased, the cascade in the system of second sound waves forms through a gradual widening of the inertial range (the shift of f_b toward higher frequencies) and a reduction in the power-law exponent m. The frequency f_b first appears as pumping surpasses the magnitude $q \sim 10$ mW cm^{-2}. The frequency f_b marking the boundary between dissipation-free energy transfer among multiple harmonics and strong dissipative losses depends on

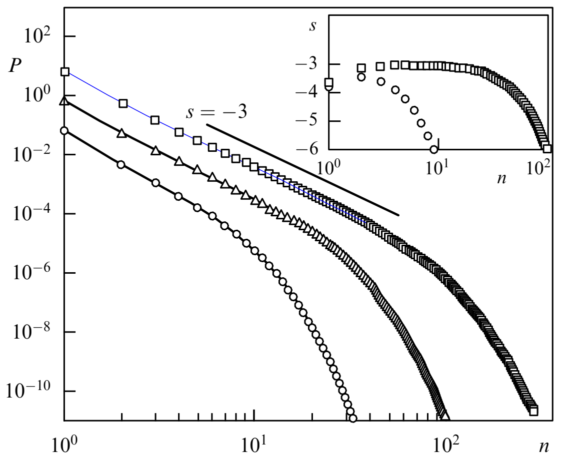

Figure 5. Energy spectra of standing second sound waves in a resonator for a monochromatic pumping with different intensities F_d: the circles correspond to $F_d = 0.01$, triangles to $F_d = 0.1$, and squares to $F_d = 1$ in relative units. The solid line is the dependence $P(n) \sim n^{-3}$. The inset shows the slope exponents of the power-law curve $P(n)$ as functions of the resonance number for the pumping levels $F_d = 0.01$ and 1.

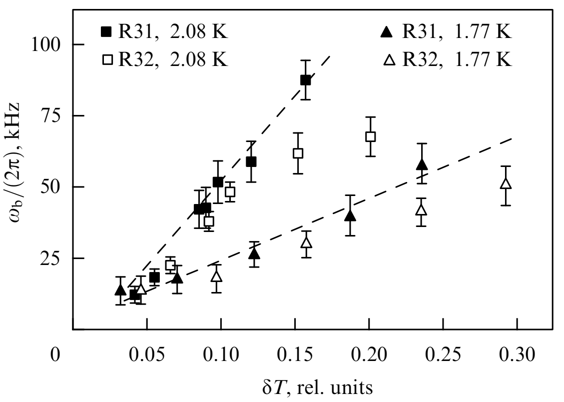

Figure 6. Dependence of the frequency at which dissipationless energy transfer between higher harmonics is superseded by viscous losses on the thermal wave amplitude in a resonator. The results for the 31st and 32nd resonances for the positive ($T = 1.77$ K) and negative ($T = 2.08$) nonlinearity coefficients.

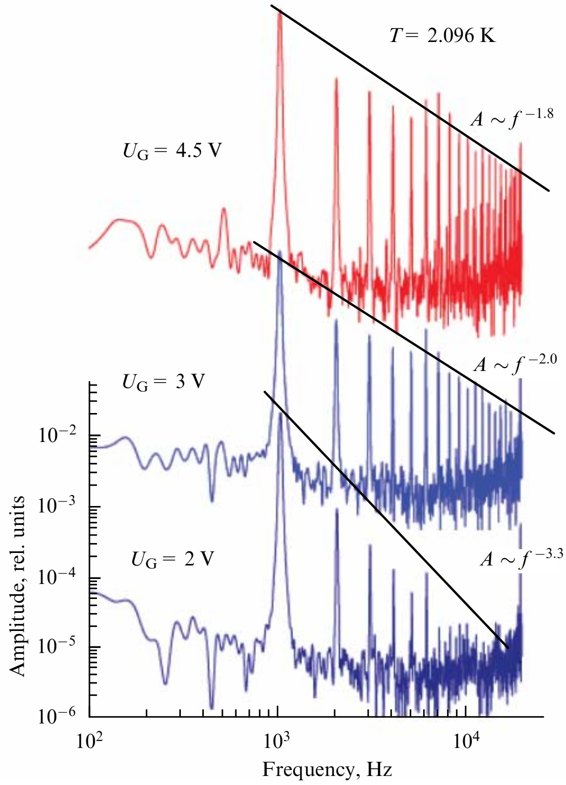

Figure 7. Formation of cascades resembling Kolmogorov ones, as pumping is increased. $T = 2.096$ K, the 11th resonance.

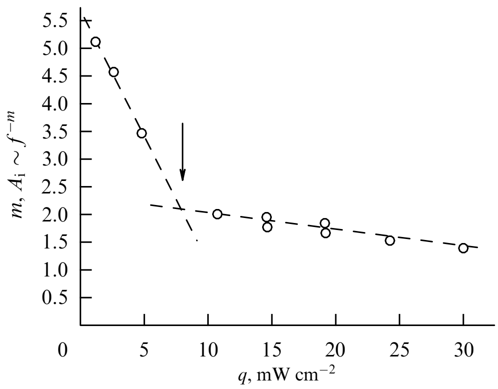

Figure 8. Dependence of the exponent m in the relation $A_i \sim f^{-m}$ for the amplitudes of multiple harmonics on the excitation intensity q for the system of second sound waves in the resonator. The change in the slope can be explained as a transition to developed acoustic turbulence. $T = 2.096$ K, the 11th resonance.

the amplitude of the principal harmonic. The dependence of f_b on A for different resonances and the nonlinearity coefficient is plotted in Fig. 6.

For the 31st resonance, the end of the inertial range for both positive and negative nonlinearity coefficients is fairly satisfactorily described by the relation

$$f_b = \mathrm{const}\,(T)\,A\,, \tag{35}$$

which corresponds to the results of theoretical analysis [103]. The deviation from the linear dependence for the 32nd resonance is determined by the possibility of generating an inverse cascade (in particular, of half the frequency) and redistributing energy fluxes toward both low and high frequencies. This mechanism is considered in more detail in Sections 5 and 8.

To learn how the intensity of the pumping signal affects the development of the turbulent cascade, we thoroughly studied the spectra of standing waves. As the intensity of the signal on the heater is increased, the number of multiple harmonics with the amplitude exceeding the noise level begins to rapidly increase (Fig. 7). In this case, the power-law exponent m in $A(f) \sim f^{-m}$ drops rapidly to $m \approx 1.5$. From Fig. 8, we can determine energy fluxes that correspond to the change in the character of energy transfer. After the heat flux reaches $q \sim 10$ mW cm^{-2}, the rapid change in the power-law exponent m is replaced by a gentle one. This same magnitude of q approximately corresponds to the crossover from a quadratic to a linear dependence of the wave amplitude in the resonator on the generator signal (see Fig. 2 and the inset in Fig. 4a).

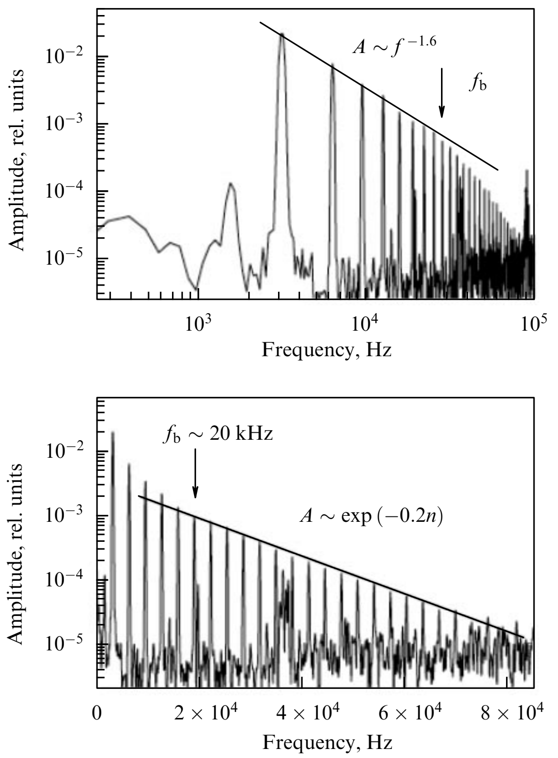

Figure 9. Typical energy spectrum for second sound standing waves in a resonator for the pumping amplitude $q \sim 12$ mW cm^{-2}, $T = 2.08$ K, the 31st resonance, $\alpha_2 < 0$, $f_{\mathrm{d}} = 3166$ Hz.

The change in the power-law exponent related to the development of a cascade of higher harmonics in the frequency domain corresponds to the regime of developed turbulence. If pumping is weak, only higher harmonics appear in the spectral space, and this can be related to a nonlinear signal distortion. In this case, the dominant interaction of higher harmonics is with the main harmonic at which the system is pumped. The increase in the pumping amplitude, by all probability, leads to the intense interaction of oppositely propagating waves in the resonator under resonance conditions and the mutual interaction of higher harmonics, which is reflected in a sharp change in the slope of the dependence $A(f) \sim f^{-m}$. Three- and four-wave interactions of counter-propagating waves should lead to a detuning between the phases of high-frequency modes and the phase of the main frequency signal, and thus a situation of developed turbulence is realized, as we show in the analysis of the shape of the high harmonic signal (see Section 6).

At high frequencies, the inertial energy flux is strongly hampered by dissipative absorption of high-frequency waves. From Fig. 9, it is seen that the power-law dependence at low frequencies is replaced by an exponential decrease in wave amplitudes for frequencies higher than 20–30 kHz. The experimental dependences of viscous absorption of high-frequency harmonics in this measurement can be described as

$$A \sim \exp(-0.2n)\,, \tag{36}$$

where $n \geqslant 6$ is the harmonic number. This behavior can be attributed to the finite viscosity of helium for wavelengths shorter than $\lambda \sim c_{20}/f_{\mathrm{b}} \sim 4 \times 10^{-4}$ m, i.e., less than several micrometers.

5. Combinative interaction of harmonic waves

The interaction of harmonics driving the developed turbulence, in addition to direct three-wave processes $\omega_1 + \omega_2 = \omega$, should also be accompanied by reverse processes $\omega_1 - \omega_2 = \omega$. A possible way to indirectly learn about the development of turbulent processes is the interaction of two frequencies of resonances whose numbers do not divide one another, for example, 31 and 9.

If the heater is simultaneously driven by signals at two resonance frequencies with different amplitudes, four standing temperature waves with different frequencies are excited there. In this case, signals at four frequencies $2\omega_1$, $\omega_1 - \omega_2$, $\omega_1 + \omega_2$, and $2\omega_2$ should appear in the spectrum of excited waves. Thus, on the excitation of the main wave with a relatively high amplitude ($U_{\mathrm{G}} = 5$ V) at the 31st resonance (31R) and an additional wave at the frequency ω_2 of the 9th resonance (9R) with a small amplitude ($U_{\mathrm{G}} = 2$ V), signals at the following resonances are excited: $\mathrm{R}18 = 2\omega_1$; $\mathrm{R}22 = \omega_1 - \omega_2$; $\mathrm{R}40 = \omega_1 + \omega_2$; and $\mathrm{R}62 = 2\omega_2$.

In addition to the dependences that correspond to arithmetic relations $2\omega_1$, $\omega_1 - \omega_2$, $\omega_1 + \omega_2$, and $2\omega_2$, we can see the appearance of combinative frequencies that correspond to the interaction of multiple harmonics with the additional frequency of the 9th resonance (Fig. 10). In Fig. 10a, we mark peaks $1+$, $2+$, formed by summing the frequencies of harmonics that are multiples of the main signal with the additional wave, and 1–, 2–, 3– are the peaks that correspond to the difference between multiple harmonics and the frequency of an additional resonance. At temperatures close to T_λ, the speed of the second sound has a strong

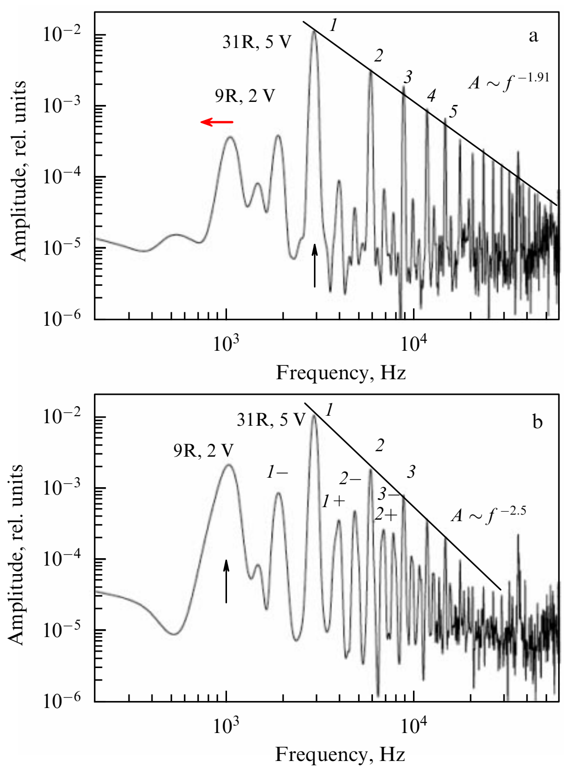

Figure 10. Fourier analysis of the signals of combinative interaction of two waves excited at the 31st ($U_{1\mathrm{G}} = 5$ V) and 9th ($U_{2\mathrm{G}} = 2$ V) resonances. The frequency of the second generator in panel (a) is somewhat detuned from the resonance frequency, but exactly coincides with it in panel (b) for the 9th resonance.

dependence on temperature, and the addition of a weak signal at the second resonance frequency from another generator slightly changes the superfluid helium temperature, which strongly shifts the resonance frequencies. Given a high Q factor, the resonator initially tuned to a maximum signal drifts out of resonance. For this reason, we used a technique whereby one of the signals (with a small amplitude) was detuned from the resonance frequency. We were able to observe how the increase in the amplitude of the additional signal (for a fixed total heat flux from the heater) modifies the character of the stationary distribution due to the main signal.

It is apparent from Fig. 10 that the increase in peaks at combinative frequencies is accompanied by an increase in the slope of the power-law dependence $A(f) \sim f^{-m}$. For particular measurements, the value of m increased from 1.9 to 2.5. Thus, the creation of additional degrees of freedom in the resonator via combinative interactions greatly suppresses the amplitudes of the direct turbulent cascade. It can be assumed that the energy flux toward the high-frequency spectral end is governed by the amplitudes of multiple harmonics, and the energies of all harmonics (the integral of the Fourier spectrum) make up this flux:

$$E = \frac{1}{2}\left(\frac{\partial C}{\partial T}\sum_{\omega} |\delta T_{\omega}|^2\right). \tag{37}$$

Integrals of spectral dependences with a developed and a suppressed turbulent cascade coincide with each other up to 2% (compare Fig. 10a and b).

That the direct turbulent cascade is suppressed in the presence of a weak additional resonant standing wave can be qualitatively explained as follows. For a somewhat augmented energy flux in the inertial range (with the added signal increasing q by less than 20%), the number of wave interactions contributing to the nonlinear process of energy transfer from low to high frequencies increases. The number of interactions per unit frequency interval then strongly increases for a fixed energy transfer per interaction act. However, a quantitative description of the suppression of the turbulent spectrum by additional excitation requires a detailed theoretical treatment.

Even if the additional perturbation is switched on, the behavior of the high-frequency end of the turbulent cascade stays practically the same, remaining exponential despite the amplitudes of harmonics being reduced by about an order of magnitude. This testifies in favor of the statement that viscous losses dominate at frequencies higher than f_{b}.

In classical nonlinear acoustics, such an interaction of waves with different frequencies is rather well known and is exploited in parametric receivers and transducers [19, 25–28]; in particular, the interaction of the 31st and 9th harmonics and the appearance of combinative frequencies close to the harmonics of the pumping wave can be interpreted in terms of classical nonlinear wave dynamics as a parametric receiver of a low-frequency signal with an intense pumping wave [104]. However, for second sound waves (thermal waves), there is one more possibility for the amplification of a weak harmonic wave: by using a constant heat flux instead of the second wave [49],

$$F(\omega) \sim I_{\mathrm{DC}} I_{\mathrm{AC}} \sin(\omega_{\mathrm{G}} t) - \frac{1}{4} I_{\mathrm{AC}}^2 \cos(2\omega_{\mathrm{G}} t), \tag{38}$$

where I_{DC} is the direct current of the heater and I_{AC} is the alternating current at the resonance frequency. Thus, two resonance frequencies are excited in the resonator, and the amplitude of the main frequency depends on the direct current magnitude. In this case, not only does the frequency of the wave generated in helium change, but also a possibility appears to amplify a weak harmonic wave by a constant heat flux. This is a specific manifestation of second sound as thermal waves.

6. Statistical properties of acoustic turbulence of second sound waves

The most important process in turbulence is the energy flow from an external source into the dissipative range of the spectrum. The energy transfer in turbulent processes is described in the framework of a cascade in spectral space. From a theoretical standpoint, the simplest case of turbulence is weak turbulence, in which waves interact with each other during a short time interval, exchanging only a small part of their energy. The interaction of wave packages is weak, and their phases are random [100, 105]. Such an approach allows using a statistical description for a broad class of external forces in the system.

An example of weak turbulence is the wave interaction in media with strong dispersion, for example, waves on a fluid surface [79, 106]. Statistical fluctuations of the velocity field in a turbulent flow are described in Kolmogorov's theory with the power-law dependence $E_k \sim k^{-5/3}$, giving the so-called $-5/3$ law (Kolmogorov cascades). For one-dimensional weak turbulence, the energy flux P determines the distribution of excitations in the frequency domain as [107]

$$n_k \sim P^{1/3} k^{-5/2} \tag{39}$$

when processes $\omega_k \leftrightarrow \omega_{k1} + \omega_{k2} + \omega_{k3}$ dominate. For weak turbulence in the inertial range, the probability density of finding waves with different amplitudes is close to the Gaussian one.

Acoustic turbulence is an example of strong turbulence, where the approach of a weak interaction of harmonic waves is not applicable. Strong turbulence is characterized by long interactions, when the interaction time is not small compared to the wave period and the energy exchange is of the order of the energy of at least one of the interacting waves [107].

For a strongly nonlinear wave in a dispersionless medium, higher harmonics are fed by the main harmonic and multiple interactions between higher harmonics, including interactions with counter-propagating waves in a resonator. It is shown theoretically that selective absorption of the frequency of a higher harmonic (or higher harmonics) dramatically slows the nonlinear energy transfer in the frequency domain and is accompanied by increased amplitudes of lower harmonics [108]. Experiments described below demonstrate to what extent the phase of higher harmonics is governed by the phase of harmonic pumping or, in other words, when the interaction of higher harmonics makes the process of energy transfer in acoustic turbulence chaotic.

We note that artificially formed saw-tooth waves, for example, a traveling strongly nonlinear harmonic wave, have a qualitatively different, ordered character of higher harmonics. In this case, energy dissipation also mainly occurs at wave discontinuities, in the range of high frequencies [109]. The energy spectrum of a saw-tooth wave is described by the dependences that are close to Kolmogorov's, $E_\omega \sim \omega^{-2}$, if multiple harmonics are in phase. The probability density for the amplitude of such a wave is constant, which is in strong contrast to the case where higher harmonics become chaotic via their interaction.

We have shown above that for a real situation observed for a system of standing waves in a resonator, a major role is played in developed turbulence by the interaction of waves not only with the main harmonic but also among themselves, including three- and four-wave interactions in counter-propagating waves. This is reflected, for example, in the generation of combinative frequencies under double pumping. In this case, both the formation of a summary wave and decay processes are possible and play a significant role. This alone is different from how the spectral dependence in the saw-tooth wave spectrum is formed. To verify the last statement, we explored the statistical characteristics of waves in acoustic turbulence under various conditions.

If pumping in a high-Q resonator is monochromatic (Fig. 11), the behavior of the first higher harmonics is governed by the energy flux from the main harmonic, and the influence of the interaction between higher-frequency harmonics on the behavior of these low-frequency modes is weak. To determine the statistical behavior of high-frequency harmonics, we filtered low-frequency signals, by successively increasing the filter frequency.

In Fig. 11, the arrows show the boundaries of successive filtering. If the initial wave is a strongly distorted harmonic wave (Fig. 12a), the successive filtering gradually makes the result more chaotic (Fig. 12b-d). For signals with a developed turbulent cascade, we computed the probability density of finding a wave with a given amplitude.

For a random variable X with any admissible value x, the probability distribution function $P(x)$ is defined as the probability of an event where the observed quantity is less than or equal to x [110],

$$P(x) = \Pr(X \leqslant x)\,. \tag{40}$$

The probability density function (PDF) is then defined as a the derivative of the probability distribution

$$p(x) = \lim_{\Delta x \to 0} \frac{P(x+\Delta x) - P(x)}{\Delta x}\,. \tag{41}$$

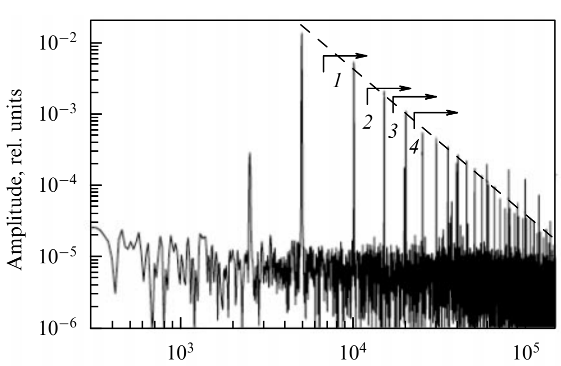

Figure 11. Amplitudes of multiple harmonics in developed acoustic turbulence. The pumping frequency f_d corresponds to the 51st resonance ($\sim$ 5030 Hz), the generator signal amplitude is $U_G = 5$ V (the heat flux $q \sim 30$ mW cm^{-2}). The arrows indicate the position of a cutoff for high-pass filtering of the recorded signal. $T = 2.08$ K, the dashed line corresponds to the dependence $A \sim f^{-2.07}$.

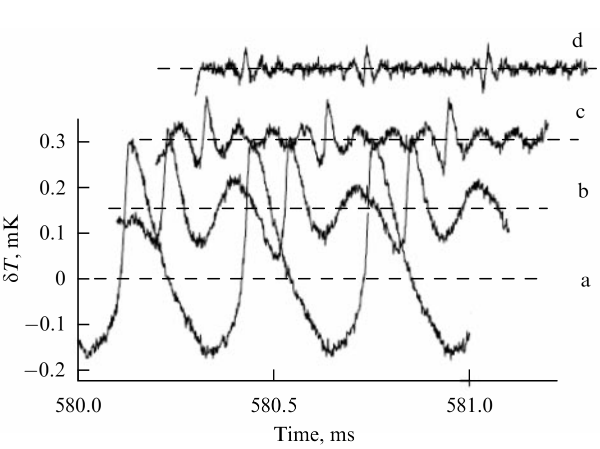

Figure 12. Second sound wave records before and after high-pass filtering. (a) The record of the second sound wave in the resonator. (b) The signal with the main harmonic removed. (c) The signal after removal of the first three harmonics; it contains the fourth and higher harmonics. (d) The signal with the first seven harmonics removed. The 33rd resonance, $f_d = 3227$ Hz, $q = 30$ mW cm^{-2}, $T = 2.08$ K.

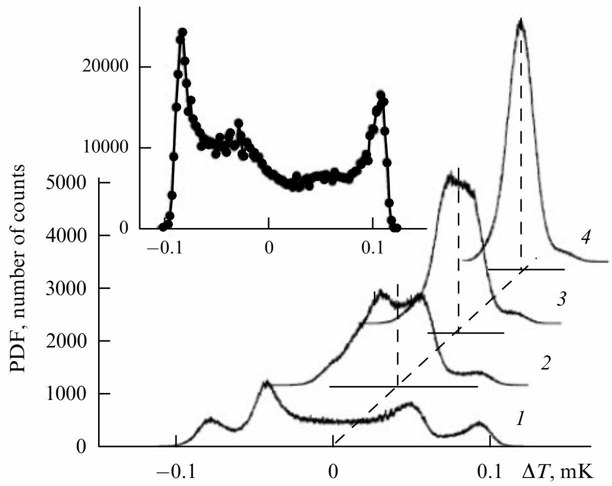

Figure 13. Change in probability density after the removal of low-frequency harmonics. The left part displays the PDF of initial signals. Curves *1–4* correspond to subsequent filtration (see arrows in Fig. 11).

In an experiment with digital signal registration, the probability density function is computed as the number of points with a given deviation from the mean.

The probability density of the signal presented in Fig. 11 upon successive filtering is plotted in Fig. 13. The probability density of the initial signal is close to the PDF of a harmonic wave. The influence of the pumping signal extends to several nearest harmonics, but disappears for higher harmonics. Filtering of low-frequency harmonics transforms the PDF of the harmonic wave into a Gaussian curve. The Gaussian PDF for higher harmonics of second sound waves always comes with a small asymmetric perturbation, which is probably related to the specifics of standing wave generation in the resonator.

The process whereby the PDF approaches the Gaussian shape depends on the degree of turbulence development and the amplitude of higher harmonics. A more developed turbulent cascade, which corresponds to a higher pumping amplitude, starts to resemble a Gaussian distribution after removing only the main harmonic, whereas for a signal with lower pumping the influence of the main harmonic also persists for higher harmonics, which can be explained by the weaker interaction of the harmonics with each other.

The influence of the interaction among harmonics outside the pumping range on the development of turbulence and chaotization of harmonics in evolving standing waves is clearly seen in the formation of combinative frequencies. The system is in this case pumped at two resonance frequencies: the main one, maintaining a turbulent cascade, and an additional one, which cannot launch a developed cascade on its own. The waves at this additional frequency can efficiently interact with the basic turbulent cascade, which gives rise to combinative frequencies (see Fig. 10).

Thus, the analysis above shows that the increase in amplitudes of the main and hence higher harmonics, extra degrees of freedom added to the system, and the interaction of waves with each other, including combinative interactions, are the reason why the PDF of high-frequency harmonics becomes progressively closer to a Gaussian distribution, characteristic of a statistically random process. As a result of such multiple interactions, a Gaussian distribution can already be observed at the stage when the second harmonic is being formed [111].

The appearance of singularities in acoustic turbulence, characteristic of random waves, indicates that acoustic turbulence in the system of second sound waves shares properties of strong as well as weak turbulence. Therefore, for such a model system in some approximation, one can use theories and approaches derived, among others, for weak turbulence; however, the effect of stochastization requires a detailed theoretical consideration.

7. Dynamics of spectra in the *k*-space in direct cascades

The problem of the formation and decay of energy cascades as energy is transferred from the range where the signal is pumped by an external force to the dissipation range plays a key role in our understanding of the physics underlying turbulence. Studying acoustic turbulence, we succeeded in experimentally exploring the formation of direct cascades upon switching on external pumping and increasing the amplitude of the main signal at the resonance frequency f_{d}. Similar experiments and temporal analyses were carried out upon switching off the external pumping.

7.1 Formation of the direct cascade

Pumping the system at a resonance frequency entails an experimental difficulty related to the change in the temperature of helium if the heater is on, and the corresponding change in the second sound propagation speed (which is particularly pronounced at temperatures close to T_{λ}, at which most of the experiments were carried out) and the resonance frequency of the system. Some experiments were carried out in the regime of switching off and on: tuning to the resonance frequency, obtaining a direct cascade, switching off the pumping signal, and then switching it on. In this case, in approximately 10 s the direct cascade decayed and the disappearance of the main harmonic was detected, but the temperature of the bath did not substantially change, and the resonance was observed at the same frequency. Similar results were obtained for a simple change in the generator frequency to off-resonance and then returning to the resonance one. The wave amplitude at the out-of-resonance frequency decayed rapidly, but the net heating of the system was unchanged.

The energy of the second sound wave is proportional to the temperature increment squared $(\delta T)^2$ [31, 32, 34]:

$$\begin{aligned}
\varepsilon &= \frac{1}{2}\,\rho_n v_n^2 + \frac{1}{2}\,\rho_{\mathrm{s}} v_{\mathrm{s}}^2\,,\\
\varepsilon &= \frac{\rho_n q^2}{2\rho\rho_{\mathrm{s}}\sigma^2 T^2}\,,\\
\varepsilon &= \frac{\rho C(\delta T)^2}{T}\,.
\end{aligned} \tag{42}$$

All subsequent discussion of the formation and decay of energy cascades are therefore carried out in terms of the squared wave amplitude A^2.

Upon switching on the generator signal under resonance conditions, the amplitude of the main harmonic, at which the system is pumped, first starts to grow. For oscillations in a resonant circuit, the process of wave formation is governed by the external force. For an ideal resonant circuit, the increase in the amplitude of oscillations in the resonator under the action of the resonance force is described by the relation

$$A(t) = \frac{F_{\mathrm{d}}}{2\gamma\omega_0}\left[1 - \exp\left(-\gamma t\right)\right]\cos\left(\omega_0 t\right). \tag{43}$$

Expanding Eqn (43) in small t gives the dependence of the form $A \sim t$. Thus, the increase in the amplitude in the initial time interval, when we can disregard the influence of damping in the system and nonlinear energy transfer in the cascade, is proportional to time. And the wave energy grows as time squared. Such an increase in energy is related to the system being pumped by an external monochromatic force.

However, the situation changes if the system is pumped keeping the energy rate constant in time, for example, if we begin to heat the system assuming a constant power of the heater. For a harmonic wave, this occurs when all the energy supplied to the heater, $Qt = \{[U_0 \sin(\omega t)]^2/R\}t$, is fully transferred to the wave. It is apparent that in this case, the growth of wave amplitude is different from that in the case of a constant force applied to the circuit. The energy in the system grows at a constant rate; hence, the wave amplitude grows proportionally to the square root of time,

$$q_{\mathrm{heater}}\, t \to \Delta E = q_0\, t + q_{0\,\mathrm{ac}}\, t = Cm\Delta T + \frac{\rho C\,\delta T^2}{T}\,V\,, \tag{44}$$

where V is the volume occupied by helium with the mass m.

With the growth in the first harmonic, more and more energy is successively transferred to higher harmonics, triggering the interaction of higher harmonics with the pumping wave and with each other; the interaction with oppositely propagating waves also evolves, and the turbulent processes described above can be observed. Thus, the type of the process changes: from a purely 'linear' one, it evolves into a 'linear–nonlinear' one, judging by the character of energy transfer. In real experiments with heat leakage from the heater into the volume of the substrate, with its continuous heating and the presence of an additional resistance at the boundary between the heater and the fluid, an intermediate situation is possible where the increase in the amplitude of the main second sound harmonic in the resonator differs somewhat from the square root dependence on the initial time interval.

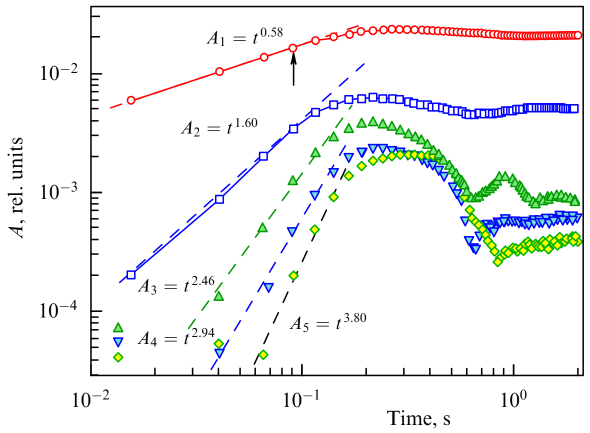

Figure 14. Growth in higher harmonics with time as pumping with a monochromatic signal at the frequency of the 18th resonance is switched on; $f_G = 893$ Hz, $U_G = 4.3$ V, and $T = 2.08$ K.

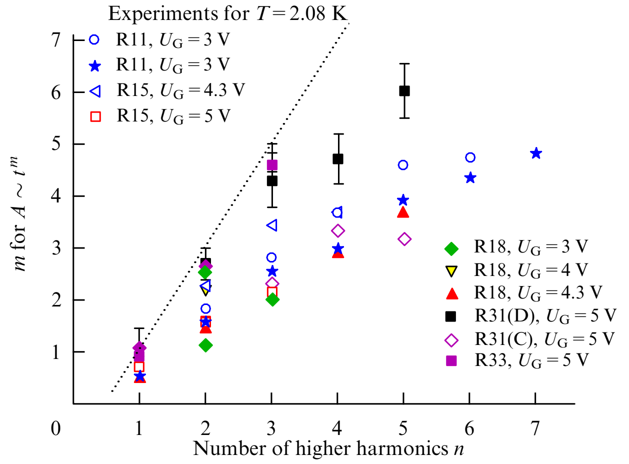

Figure 15. Experimental dependences of the slope on the time growth curve for higher harmonics in a nonlinear wave. The data for a set of experimental studies are given. The dotted line is the dependence $m = 1 + 2(n-1)$, $T = 2.08$ K.

Experimental possibilities for recording long signals and low speeds of second sound waves allowed us to study the dynamics of the formation of energy cascades in turbulence developing in the resonator. Figure 14 plots the measurement results showing the growth in higher harmonics. From the figure, it can be seen how higher harmonics successively grow, acquiring energy from lower-frequency modes. They closely follow a power law. In this experiment, the power-law growth of harmonics continues for 0.1 s after the pumping signal is switched on, and this time depends on the pumping amplitude and on the amplitude of the wave forming at the pumping frequency, for which nonlinear energy transfer into higher harmonics begins to dominate over linear losses. This transition occurs when the acoustic Reynolds number reaches unity, $\mathrm{Re}_{ac} = \alpha\delta TQ \geqslant 1$. This condition is achievable for high-quality resonators. In low-quality resonators, the wave amplitude does not reach critical values, and all the energy pumped in the resonator is converted into linear losses, $\mathrm{Re}_{ac} = \alpha\delta TQ < 1$.

The growth in the amplitude of the main resonance at the initial stage follows a time dependence close to $A_1 \sim \sqrt{t}$. The growth in higher harmonics in the experiment is described by a dependence close to

$$A_n \sim A_{n-1}\, t \sim t^{1/2+(n-1)} \,. \tag{45}$$

Figure 15 presents the data obtained in experiments exploring the formation of the direct cascade of second sound waves. Even with the scatter in the experimental points, the index of the power-law function is close to that in dependence (45). From a physical standpoint, this implies that the growth in the amplitude of the nth harmonic is governed by the amplitude of the preceding harmonic, but it takes some time to transfer energy from the $(n-1)$th harmonic to the nth harmonic, which means that higher harmonics in the resonator have inertial properties. Thus, the increase in the energy of the nth harmonic can be expressed as $E_n \sim E_{n-1}\, t^2$.

To determine the temporal dependence of harmonics growing higher, we performed computer simulations of energy transfer in interactions of harmonics with a linear dispersion relation $k \sim \omega$. The following model of interaction was adopted: two interacting waves with frequencies ω_1 and ω_2 form a wave $\omega_1 + \omega_2 \to \omega_3$ with some probability.

Computations were carried out under the assumption that the probability of merging into a wave with the frequency ω_3 depends on the energies of waves with ω_1 and ω_2. There is no damping in the inertial range, but at the 150th resonance the energy flux disappears: the range of total energy dissipation begins, where all wave decay processes $\omega_3 \to \omega_1 + \omega_2$ cease. All the energy injected into the system is transferred to the growth of amplitudes of all interacting harmonics, up to the 150th, and part of the energy is lost through the right end of the spectrum. Stationary values of amplitudes under these conditions are close to the observation results [92].

Computations carried out by Kolmakov [112] under the assumption of a constant force acting on the resonator lead to the following behavior of growth of the amplitudes with time:

$$A_i \sim t^{1+2(i-1)} \,. \tag{46}$$

This behavior is shown in Fig. 15 by the dotted line. It can be seen that the experimental dependences are closer to (45) than to (46).

7.2 Decay of the direct cascade, the ‘linear’ and ‘nonlinear’ times

When exciting harmonic signals in a resonator, part of the energy is removed by linear losses related to the dissipation of the harmonic wave, and the remaining part feeds the energy transfer to higher harmonics. This energy transfer determines the ‘nonlinear’ time — the time during which energy is transferred from the pumping frequency to the second and higher harmonics. The ‘linear’ time can be found experimentally from the resonator Q factor by exciting the resonator with a low-intensity wave. Nonlinear energy transfer to higher harmonics is characterized by smaller times of energy loss in the resonator. This reasoning laid the foundation for studies of the temporal evolution of the frequency spectrum after the pumping is switched off.

The results of exploring the Q factor of the resonator as a function of the pumping amplitude and the temporal dependence of the decay of the oscillation amplitude are plotted in Fig. 16.

The quality of the resonator was defined as the width of the resonance curve at the height $A_{max}/\sqrt{2}$. For small

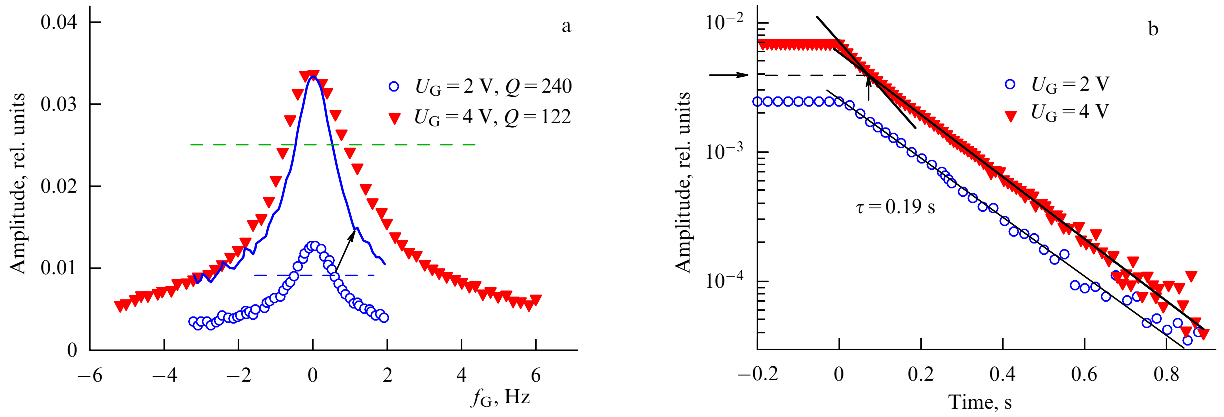

Figure 16. (Color online.) (a) Influence of pumping amplitude on the resonator Q factor; the shape of resonance curves for the excitation amplitudes $U_G = 2$ V and $U_G = 4$ V. The blue line shows the resonance excitation curve $U_G = 2$ V at a zoomed-in scale. (b) Time dependence of the signal amplitude in the resonator when the pumping is off for the initial excitation amplitudes $U_G = 2$ V and $U_G = 4$ V, the 7th resonance, $T = 2.08$ K.

excitations, the Q factor is governed only by the physical properties of the resonator (linear attenuation processes). An increase in the signal amplitude leads to nonlinear energy transfer to higher harmonics. The Fourier analysis in this case shows the growth in the amplitude of higher harmonics in a distorted second sound wave, accompanied by a decreasing resonator Q factor.

Switching off the pumping for small amplitudes of oscillations leads to their exponential decay

$$A(t) = A_0 \exp(-\gamma t) \sin(\omega_d t + \varphi_0)\,, \qquad (47)$$

where γ is the attenuation coefficient and ω_d is the oscillation frequency of the resonator with damping. The decay time scale τ, found from the resonator Q factor $Q = 240$ for a given resonance frequency (Fig. 16a) as $\tau = 1/\gamma = 2Q/\omega_d = 0.22$ s, is close to the value measured by the oscillation decay time $\tau = 0.19$ s (Fig. 16b).

The resonator Q factor measured at large excitation amplitudes is substantially lower, which is related to the nonlinear wave distortion. This is seen in the time dependences of oscillations fading away in the resonator as changes in the characteristic signal decay times at large and small oscillation amplitudes ($\tau_{high} = 0.085$ s and $\tau_{low} = 0.19$ s, respectively). The reduction in the signal level below the position marked with the arrow leads to a noticeable reduction in nonlinear transfer to higher harmonics, leaving only the losses related to the resonator Q factor at the pumping frequency: the slope of exponential decay coincides with the slope of decay in the resonator at a small signal amplitude (the curve for $U_G = 2$ V).

We explored the temporal characteristics of decay processes in more detail for the 11th resonance, where the resonator Q factor is very large ($Q = f_R/\Delta f \approx 3900$), which allowed observing very long oscillation decay times.

We analyzed a signal with a duration of 20 s, stored numerically by time intervals to clarify the behavior of higher harmonics upon switching off the pumping (Fig. 17). During the analysis, it was possible to follow the change in amplitudes of at least 10 multiple harmonics. When the external pumping is off, the energy losses of the main harmonic, which was directly pumped, follows two channels: that of linear damping and that of nonlinear energy transfer in higher harmonics.

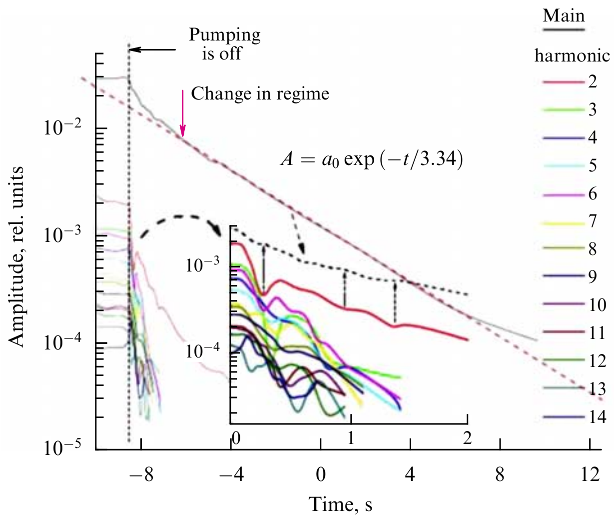

Figure 17. (Color online.) Time dependence of amplitudes of multiple harmonics for signal decay. The 11th resonance, $f_G = 516.81$ Hz, $T = 2.08$ K, $U_G = 3$ V, which corresponds to $q = 10.8$ mW cm^{-2}. The inset shows the initial moment after pumping was stopped. The dashed line in the inset is the scaled dependence of the amplitude of the main harmonics.

The process of energy flux redistribution between the nearest harmonics after pumping is switched off leads to chaotic changes in amplitudes of higher harmonics. It is noteworthy that a sharp reduction, for example, in the second harmonic causes a reduction in the decay rate of the main harmonic (arrows in Fig. 17), i.e., the process of energy transfer between the neighboring harmonics depends not only on the difference between the energies of these modes but also on some inertial component: an increase in the amplitude (and the energy of a given mode, e.g., the second harmonic) takes a time of the order of several tenths of a second. If this inertial time is different for different harmonics, this naturally leads to a chaotic change in respective amplitudes as they fade away.

The chaotic behavior of higher harmonics continued for 1–1.5 s, which corresponds to approximately 1500 periods of the main harmonic; the higher harmonics were indistinguishable later. Their extinction begins from high frequencies: the second and then the main harmonic disappear last. Similar behavior was observed experimentally in the decay of capillary waves on the surface of liquid hydrogen [101].

This behavior differs from theoretical predictions for processes characteristic of weak turbulence [100], where a situation is possible when the energy flux is conserved and the spectral peak moves from low to high frequencies. For example, oscillations of a capillary wave can continue long after gravity waves have disappeared.

After approximately 2 s, the energy flux from the main harmonic to higher harmonics becomes negligibly small; higher harmonics disappear and the main harmonic decays with a characteristic time τ_L. The decay time τ_L in Fig. 17 corresponds to a resonator with the Q factor $Q \sim 5400$. This value is approximately 40% higher than the measured Q factor of the 11th resonance for the pumping signal $U_G = 2$ V, which points to the presence of a nonlinear process for such pumping ($Q_{NL} < Q_L$). 'Linear' decay lasts for at least 10 s ($\geqslant 10{,}000$ oscillations at the pumping frequency).

If we assume that linear and nonlinear processes are additive, the main harmonic energy losses can be represented as

$$\Delta E_{\mathrm{main}} = \Delta E_L + \Delta E_{NL} . \tag{48}$$

In this case, the linear time, which is determined from the decay of oscillations after $t = 2$ s, is $\tau_L \approx 3.3$ s. For the 'linear' decay, we then have

$$A_{\mathrm{main}}(t) \approx A \exp\left(-\frac{t}{\tau_L}\right) . \tag{49}$$

Accounting for energy balance (46), the difference between the observed decay of the main harmonic and the extrapolated 'linear' decay is determined by the nonlinear energy flux to higher harmonics, beginning from the second,

$$A^2_{NL}(t) = A^2_{\mathrm{main}}(t) - A^2_L(t) \sim \exp\left(-\frac{2t}{\tau_{NL}}\right) . \tag{50}$$

This difference is depicted in Fig. 18. Initially, the reduction in the amplitude of the main harmonic is governed only by the energy flux to higher harmonics, and 'linear' losses are small

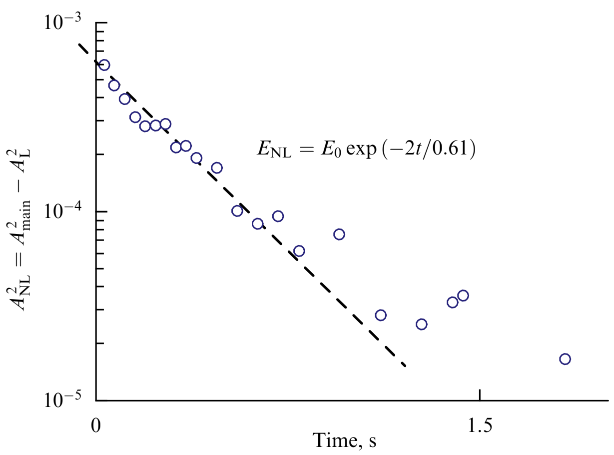

Figure 18. Energy of the 'nonlinear' oscillation decay defined as the difference between the energy of oscillations of the main harmonic and extrapolated 'linear' damping.

in its background,

$$A_{\mathrm{main}}(t) \sim A \exp\left(-\frac{t}{\tau_{NL}}\right) . \tag{51}$$

An estimate shows that the nonlinear time is almost an order of magnitude smaller than the linear one ($\tau_L \approx 3.3$ s and $\tau_{NL} \approx 0.6$ s).

8. Inverse wave cascades

Second sound waves have a linear dispersion relation, and their interactions must respect the conservation of energy $\omega = \omega_1 + \omega_2$ or $\omega + \omega_1 = \omega_2 + \omega_3$ and momentum $k = k_1 + k_2$ or $k + k_1 = k_2 + k_3$ for three- and four-wave processes. Nearly plane waves in the resonator are collinear, and for such waves the generation of multiple harmonics follows automatically from the linear dispersion relation

$$\omega_1 + \omega_2 \to \omega_3 . \tag{52}$$

However, for collinear waves, with some probability given by (32), the inverse process is possible in addition to the direct process, according to the linear balance equation (31),

$$\omega_1 \to \omega_2 + \omega_3 . \tag{53}$$

Such an inverse process can lead to the formation of two waves with equal or different frequencies from the wave at the frequency at which the energy is pumped into the system. An inverse cascade can develop in this case, carrying energy to the low-frequency spectral edge instead of the high-frequency one.

8.1 Inverse energy cascade as a wave decay process

The formation of an inverse cascade means the excitation of frequencies lower than the pumping frequency in the resonator spectrum. Such a situation is possible for the enstrophy flux in two-dimensional geometry, given by a contour integral for vector fields of a vortical system, when small eddies can merge into large vortices [113]. In this case, energy is also transferred to the high-frequency spectral end, where it is removed by viscosity, but vorticity can be transferred to the low-frequency end. In the one-dimensional geometry, given potential wave fields, the formation of vortices is impossible by definition, and therefore in one-dimensional (or quasi-one-dimensional) acoustic turbulence, only potential flows and transitions between frequencies of wave modes are possible, together with the associated energy flows in spectral space, the direct and inverse energy cascades.

For plane waves with the linear dispersion relation, in addition to decay process (53), two waves of the main harmonic can interact, forming two mutually complementing oscillations [114]:

$$\omega_{k_0} + \omega_{k_0} \to \omega_{k_0+k} + \omega_{k_0-k} . \tag{54}$$

For a linear dispersion relation, Eqn (54) can be rewritten as $2\omega \to \omega_1 + \omega_2$, where $\omega_1 = \omega + \Delta\omega$ and $\omega_2 = \omega - \Delta\omega$. The inverse cascade can evolve via three-wave (53) and four-wave (54) processes.

The inverse cascade was observed in several numerical experiments that model wave behavior under different conditions, in particular, the behavior of a surface gravity wave on water [115–117]. The first experimental observation of the inverse cascade was apparently that in Ref. [118].

8.2 Inverse cascade, stationary regime

The generation of subharmonics in a discrete resonant circuit (resonator) is possible only if there are sufficiently many degrees of freedom at frequencies smaller than the pumping frequency, and, as indicated by the experiments described below, if the pumping signal exceeds some threshold value close to that at which nonlinear effects dominate in wave interactions.

If pumping is at the 51st resonance, a large number of subharmonics are generated, and peaks of the inverse cascade approximately match the resonances indicated in Fig. 19. Experimental studies have shown that inverse cascade spectra are formed under a detuning from the resonance frequency toward higher frequencies. An example of such a development of the inverse cascade is given in Fig. 20.

Attempts to relate the development of the inverse cascade to the sign of the nonlinearity coefficient and nonlinear behavior of waves in the resonator failed to explain the direction of the frequency shift needed to trigger the inverse cascade. Indeed, the nonlinear dependence of the wave propagation speed bends the resonance dependence [119], and for $\alpha_2 Q \delta T > 1$, the resonance curve bifurcates: three different amplitudes correspond to one frequency.

With increasing the signal amplitude, the resonance curve becomes asymmetric and acquires a discontinuity from the high-frequency side. However, the generation of the inverse cascade in experiments proves to be unrelated to the nonlinearity coefficient. For the temperature $T = 2.08$ K, the nonlinearity coefficient is negative, and therefore the resonance curve should bend toward lower frequencies, $f = (c_{20} + \alpha_2 \delta T)/(2L)$, which is not observed experimentally. Moreover, the change in the nonlinearity sign to positive (experiments at $T = 1.7$ K) gives the same effect: the inverse cascade is observed only if the pumping frequency is biased toward higher frequencies from the resonance curve maximum. Thus, it is quite obvious that the observed effect is related to nonlinear wave behavior (the threshold character of the effect), but conditions for its appearance (frequencies of pumping the system) are not governed by the nonlinear properties of the wave in a resonator.

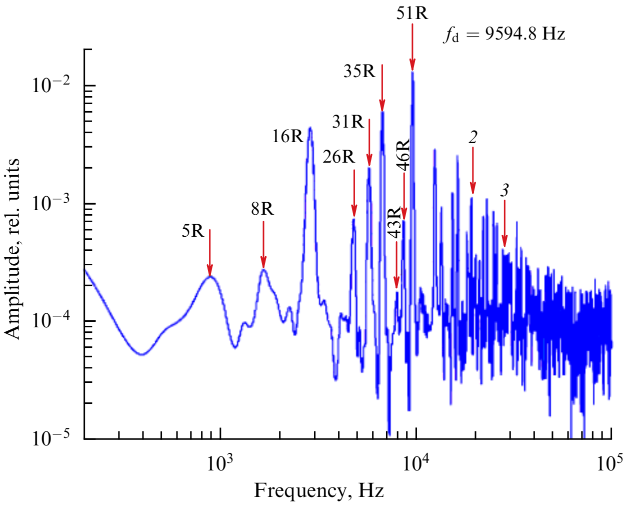

Figure 19. Frequencies of developed turbulent cascades for pumping at the frequency of the 51st resonance; the pumping frequency is $f_d = 9594.8$ Hz. The numbers with R are those of the resonances; *2* and *3* denote the positions of multiple harmonics of the main frequency. $T = 2.079$ K, with a negative nonlinearity coefficient.

The onset of the inverse cascade of second sound waves in superfluid helium is defined by a set of conditions:

- Wave generation in the resonator should occur at resonances with large numbers to ensure sufficiently many degrees of freedom at low frequencies;
- The intensity of the pumping wave should exceed the value above which nonlinearity begins to play an essential role in wave interactions in the system (approximately, $q \geqslant 6-10$ mW cm^{-2});
- To have the inverse cascade, a frequency shift toward frequencies higher than the resonance frequency by a small increment of the order of $\Delta f \approx 2$ Hz is needed.

The formation of the inverse cascade is always characterized by a time delay in the development of subharmonics, which can take up to several dozen seconds, and by a frequency hysteresis of this process. When the pumping frequency was varied above the main resonance frequency, the inverse cascade existence domain, the number of subharmonics and their amplitudes were strongly dependent on the direction and speed of the frequency change. The time the inverse cascade began to evolve was also dependent on the frequency offset from the resonance.

The origin of the frequency offset from the resonance maximum can be explained by the frequency properties of the resonator. According to the measurements, the dependence of resonance frequencies on the resonance number has the form $\omega_n = \omega_0 n + \Delta\omega$ (where $\Delta\omega \approx 2$ Hz), whence it follows that a small frequency shift toward higher frequencies allows the resonance conditions to be exactly satisfied at smaller numbers:

$$\omega_d + \Delta\omega = (\omega_0 n_d + \Delta\omega) + \Delta\omega$$
$$= (\omega_0 n_1 + \Delta\omega) + (\omega_0 n_2 + \Delta\omega) = \omega_1 + \omega_2 \,. \quad (55)$$

Thus, the conditions for the formation of the inverse cascade in the one-dimensional geometry are as follows:

- sufficiently many degrees of freedom in the low-frequency domain of discrete spectral space (for the resonator);
- collinear arrangement of wave vectors for a linear dispersion relation;
- sufficiently large amplitude of the pumping signal for the manifestation of nonlinear wave interactions;
- frequency shift by some value determined by the details of the resonator frequency response.

8.3 Formation of the inverse cascade

To answer the question about the nature of the inverse cascade, we experimentally explored the processes pertaining to the inverse cascade formation and fading; with this aim, the technique of cutting the signal into time intervals and performing a frequency analysis for each interval was used, enabling us to study the temporal behavior of higher harmonics and subharmonics. Figure 21 shows results of a temporal signal analysis.

At the time moment $t = 0$, the signal was switched to the inverse cascade formation frequency close to the 51st resonance. We can clearly see a well-developed direct cascade with multiple harmonics, the amplitudes of the second and third being denoted as R102 and R153. After 10 s, the subharmonics start to evolve; in this example, they corre-

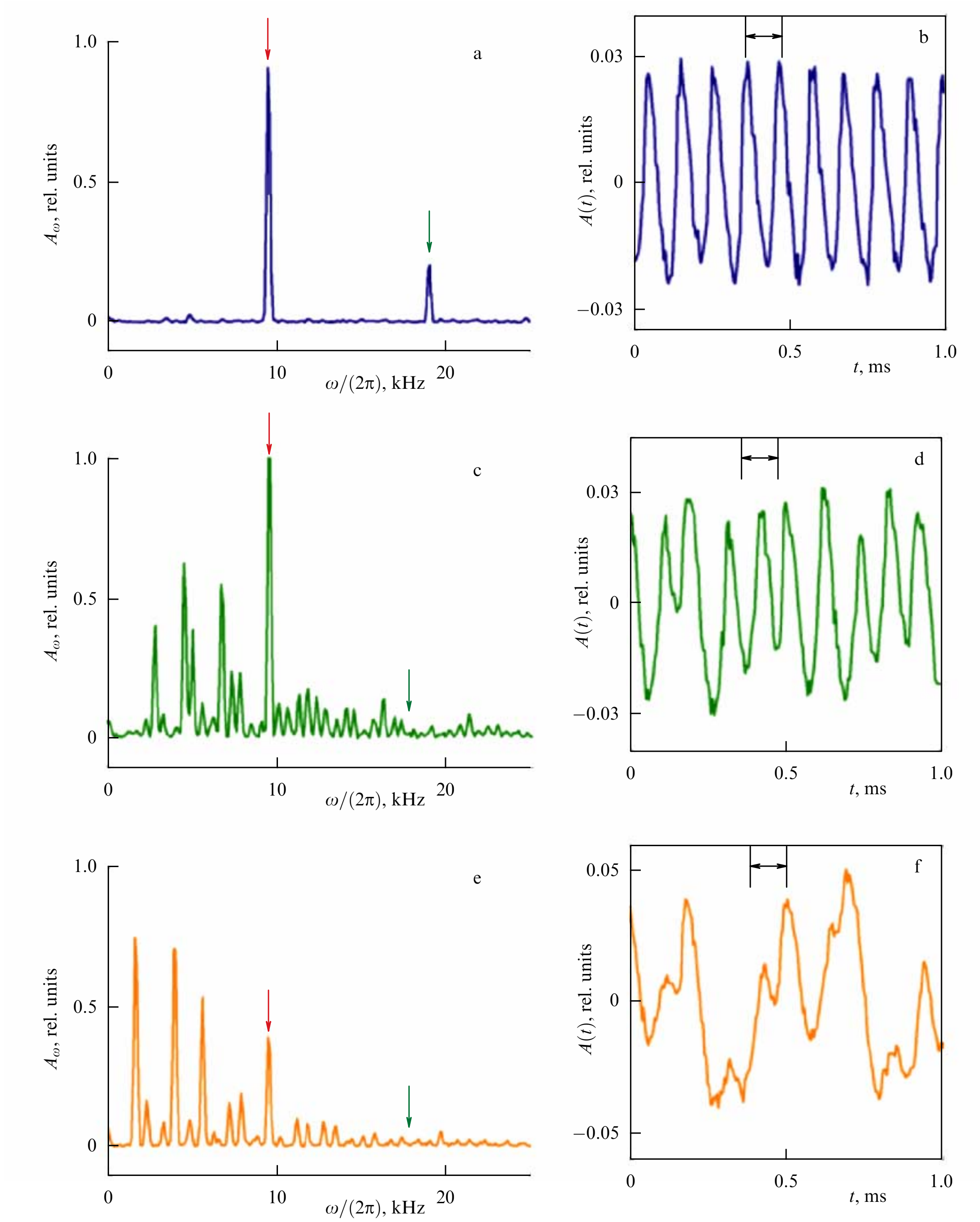

Figure 20. (b, c, e) Evolution of the shape of the observed signal of a standing wave in a resonator and (a, d, f) its spectrum for a small detuning of ω_d close to the 96th resonance: $\omega_\mathrm{d}/(2\pi) = 9530.8$ Hz (a, b), 9532.4 Hz (c, d), and 9535.2 Hz (e, f). The heat flux is $q = 42$ mW cm^{-2}, $T = 2.08$ K, with a negative nonlinearity coefficient. The main harmonic and its first higher harmonic are marked in panels a, c, e by vertical arrows. The horizontal arrows in panels b, d, f correspond to the period of the main harmonic.

spond to the 35th and 16th resonances. The amplitudes of all harmonics of the direct cascade begin to decrease. After 40 s, a pair of 24th and 27th resonances appears. It is clearly seen that the resonances evolve pairwise and that the sum of their frequencies corresponds to that of the main harmonic.

These experiments confirm that subharmonics occur in correlated pairs, which points to the decay character of the inverse cascade spectrum,

$$\omega_\mathrm{d} \to \omega_1 + \omega_2\,, \tag{56}$$

with the appropriate conditions for frequencies and amplitudes. Further, the subharmonics interact with each other, scattering on each other, interacting with higher harmonics, and forming combinative frequencies due to interactions with the main and multiple harmonics. This is clearly seen from the Fourier analysis, which reveals a broad row of frequency peaks between multiple harmonics of the direct cascade. However, we are at present not in a position to make an unambiguous statement about turbulent interaction in the inverse cascade.

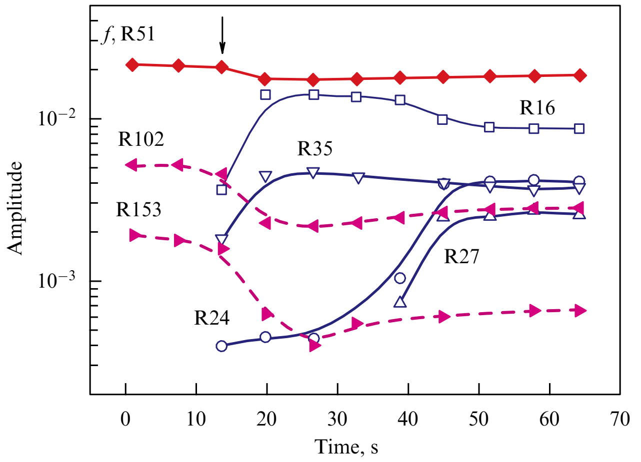

Figure 21. Formation of multiple harmonics and subharmonics when the inverse frequency cascade is excited. The 51st resonance, $q = 30\ \mathrm{mW\ cm^{-2}}$, $T = 2.08$ K.

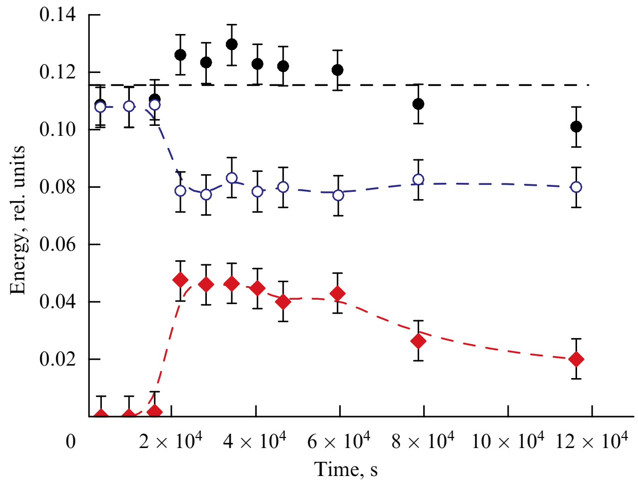

Figure 22. Energy integral during the inverse cascade development: light circles show the energy in the direct cascade, diamonds show the energy in the inverse cascade, black dots are the sum of energy of all harmonics except the main one. The results were obtained by processing data from Fig. 21. The 51st resonance, $q = 30\ \mathrm{mW\ cm^{-2}}$, and $T = 2.08$ K.

8.4 Decay of the inverse cascade

Our experimental technique allows us to explore the decay of stationary spectra for ranges of higher harmonics and subharmonics. Observing the dependence on time, we can conclude that for the inverse cascade, just as for the direct one, switching off the external pumping leads to the decay of the spectrum beginning from the high-frequency end. The decrease in the energy flux induces a chaotic change in the amplitudes of all harmonics. The last to 'ring' in the decaying developed inverse cascade is a subharmonic with the initially large amplitude for which the system's Q factor was sufficiently high.

Indeed, in experimental studies of the decay of oscillations in a system with a developed inverse cascade and the pumping frequency at the 96th resonance ($f_G = 4715$ Hz), it was found that as the main harmonic fades, one of the intense subharmonics takes over, in this case, the subharmonic with the frequency $f \sim 2900$ Hz. This is an argument in favor of the statement that the energy cascade decays from the high-frequency spectral end. Without pumping, only interactions between harmonics persist. The energy flux is damped at each harmonic, and is transferred by the harmonics because of the nonlinear wave interaction into both the high-frequency part of the spectrum (summation of frequencies) and its low-frequency part (a wave decay process). To quantitatively describe the process of inverse cascade decay, we need an adequate theoretical model of energy transfer into the low-frequency spectral range, which is currently missing.

8.5 Energy fluxes in the inverse cascade

One interesting question concerning the inverse cascade is related to the direction of the energy flux: does the energy flux remain unchanged in the high-frequency domain or is the energy pumped into the system divided between direct and inverse processes? It is quite possible that the subharmonics in the inverse cascade, once excited, stay in equilibrium with the energy of the main harmonic, at which the excitation energy is pumped into the system. For example, in a river, the presence of a dam does not influence the total flux of water at a given location, which is determined only by net runoff from external sources.

We can compute the total energy in the direct and inverse spectrum as integrals of the amplitudes of Fourier components over the ranges of small ($f < f_d$) and large ($f > f_d$) frequencies. It can be assumed that the energy flux entering the system determines the total energy of all harmonics in the inertial range. When combinative waves were excited in the system by pumping it with two resonance signals (see Section 5), the direct cascade was suppressed. However, this suppression had no impact on the common energy in the cascade, which implies a correlation between the total energy in the harmonics and the spectral energy flux. Results of exactly such computations of the net energy for all harmonics during the development of the inverse cascade are given in Fig. 22.

The growth in the subharmonics of the inverse cascade (after 20 s) leads to an increase in energy in the low-frequency wing of the spectrum. At the same time, the energy in the right-hand part of the spectral cascade decreases. However, the total energy over the entire spectrum is practically unchanged. This indicates that the energy flux becomes redistributed between the high- and low-frequency parts of the spectrum. If the inverse cascade had no energy flux, then the total energy in the right-hand part of the spectrum would be unchanged, as in the case where the system is pumped at two resonant frequencies.

There is still a question of energy dissipation in the low-frequency spectral domain. We recall that the resonator Q factor depends on the frequency of waves excited in it. And the lower the number of a resonance is, the lower the Q factor. Thus, energy transferred to the low-frequency spectral domain is effectively lost via viscous friction against the walls, which becomes larger as the frequency of standing waves decreases.

Thus, experiments indicate that during the formation of the inverse cascade, energy is indeed transferred into the high-frequency range, where it decays on bulk viscosity and (or) geometric irregularities, as well as into the low-frequency range, where friction against the walls is substantial and the system Q factor is small compared to that at high frequencies.

After all, the nature of dissipative processes does not play a fundamental role: the occurrence of fluxes of energy pumped into the system by an external source and transferred to the regions of high as well as low frequencies is discovered experimentally.

9. Conclusions

Experimental studies of acoustic turbulence of second sound waves in superfluid helium are based on the unique properties of helium: its extraordinarily small viscosity (and hence weak damping for temperature waves) and anomalously high nonlinearity coefficient α_2, which, furthermore, can change sign if the temperature of superfluid helium is varied, taking values from $\alpha = -\infty$ close to T_λ to large positive values at temperatures lower than $T_0 = 1.88$ K, at which $\alpha_2 = 0$. The experiments carried out in a resonator of second sound waves enabled us to explore the specifics of energy transfer in the spectral domain and the formation and decay of spectral cascades. Both direct and inverse energy fluxes were discovered, directed from the pumping range to the dissipation range at the high-frequency edge of the spectrum (the direct cascade) and to the low-frequency part (the inverse energy cascade). The energy flux was created by nonlinear processes in initially harmonic waves.

It has been found experimentally that for quasi-one-dimensional acoustic turbulence, the processes of interaction of higher harmonics in the direct cascade are strongly amplified in a resonator with a Q factor of the order of several thousand for the net heat flux power $q \geqslant 10\,\mathrm{mW\,cm^{-2}}$. This is reflected in the formation of the inertial energy transfer range in the spectral domain, and in interactions between higher harmonics and counter propagating waves forming standing waves under resonance conditions, which is described in terms of random processes for higher harmonics of the energy cascade.

The power-law dependence of amplitudes of multiple harmonics in the inertial range is $A(f) \sim f^{-m}$ with $m \sim 1.5$. The end of the inertial range for both positive and negative nonlinearity coefficients is rather satisfactorily described by the relation $f_\mathrm{b} = \mathrm{const}\,(T)A$, where A is the pumping amplitude, which agrees with the results of theoretical analysis.

As we have shown, the formation of higher harmonics in acoustic turbulence of second sound waves in superfluid helium follows the dependence $A_n \sim A_{n-1}t \sim t^{1/2+(n-1)}$, which can be explained in the framework of the model of pumping at a constant power.

The study of decay of turbulent processes upon switching off the pumping allowed us to separate linear and nonlinear decay times for oscillations in a system of standing second sound waves, which are governed by the Q factor of the resonator (linear time) and the rate of spectral energy transfer to higher harmonics (nonlinear time). The linear time proved to be much larger than the time of energy transfer in the spectral domain, which imposes substantial limitations on the conditions enabling the observation of the acoustic turbulence of second sound waves in a resonator: a resonator with a high Q factor is required to ensure that $\tau_\mathrm{L} \gg \tau_\mathrm{NL}$.

We have shown that the formation of the inverse cascade is governed by decay processes of a pumped wave; in this case, the energy of pumping, remaining constant, is split into two fluxes, supplying the high- and low-frequency parts of the spectrum.

However, not all observed phenomena are described theoretically. For example, stochastization of higher harmonics in interactions of counter-propagating nonlinear waves in a resonator and the dynamics of the formation and decay of inverse and direct cascades are understood qualitatively, but their quantitative description requires appropriate theories. One motivation of this review was to attract the attention of theoreticians to available experimental results.

The research carried out illustrates a series of feasible tasks from the standpoint of studying strongly nonlinear interacting waves in a high-Q resonator using the example of second sound waves in superfluid helium. In particular, one can explore the generation of standing resonant waves pumped by noise, the interaction between nonlinear waves and noise in a resonator, and the formation and decay of energy cascades in nonlinear waves interacting with noise. Yet another problem arising in studies of this system is the interaction of nonlinear waves (potential perturbations) and controlled vortex features (quantum vortices), which also opens broad perspectives for theoretical models.

Acknowledgments

The author is indebted to researchers at the Institute of Solid State Physics (ISSP) RAS, L P Mezhov-Deglin and G V Kolmakov, who coauthored the main studies on acoustic turbulence, A N Ganshin and P V E McClintock, collaboration with whom enabled the main experiments to be carried out, A A Levchenko, V V Lebedev, E A Kuznetsov, and participants of the seminars 'Physics of low temperatures' and 'Wave phenomena' of the ISSP RAS for numerous helpful discussions. The author is also indebted to A V Lokhov for the help in carrying out experiments, and the personnel of the cryogenic service team at the ISSP RAS, who maintained the capacity to work with liquid helium. The author acknowledges support through Engineering and Physical Sciences Research Council grants for the opportunity to carry out part of the experimental work at the University of Lancaster. The work was performed in the framework of a state assignment; the analysis of temporal characteristics of transient processes in the formation of direct and inverse cascades and of characteristics of resonators was carried out with the support of the Russian Science Foundation grant 14-22-00259.

References

1. Monin A S, Yaglom A M *Statistical Fluid Mechanics* Vol. 1 (Cambridge, Mass.: MIT Press, 1971); Translated from Russian: *Statisticheskaya Gidrodinamika — Mekhanika Turbulentnosti* Vol. 1 (Moscow: Nauka, 1965)
2. Monin A S *Sov. Phys. Usp.* **21** 429 (1978); *Usp. Fiz. Nauk* **125** 97 (1978)
3. Riman B *Sochineniya* (Works) (Moscow: Gostekhizdat, 1948)
4. Bateman H *Mon. Weather Rev.* **42** 163 (1915)
5. Burgers J M *Proc. R. Neth. Acad. Sci.* **43** 2 (1940)
6. Burgers J M *Adv. Appl. Mech.* **1** 171 (1948)
7. Burgers J M *The Nonlinear Diffusion Equation: Acymptotic Solutions and Statistical Problems* (Dordrecht: D. Reidel, 1974)
8. Kadomtsev B B, Karpman V I *Sov. Phys. Usp.* **14** 40 (1971); *Usp. Fiz. Nauk* **103** 193 (1971)
9. Rudenko O V, Soluyan S I *Theoretical Foundations of Nonlinear Acoustics* (New York: Consultants Bureau, 1977); Translated from Russian: *Teoreticheskie Osnovy Nelineinoi Akustiki* (Moscow: Nauka, 1975)
10. Rudenko O V *Sov. Phys. Usp.* **29** 620 (1986); *Usp. Fiz. Nauk* **149** 413 (1986)
11. Tritton D J *Physical Fluid Dynamics* 2nd ed. (Oxford: Oxford Univ. Press, 1988)
12. Gurbatov S N et al. *J. Fluid Mech.* **344** 349 (1997)
13. Bec J, Frisch U, Khanin K *J. Fluid Mech.* **416** 239 (2000)

14. Davidson P A *Turbulence*: *An Introduction for Scientists and Engineers* (Oxford: Oxford Univ. Press, 2004)
15. Noullez A et al. *Phys. Rev. E* **71** 056305 (2005)
16. Bec J, Khanin K *Phys. Rep.* **447** 1 (2007)
17. Gurbatov S N, Rudenko O V, Saichev A I *Volny i Struktury v Nelineinykh Sredakh bez Dispersii. Prilozheniya k Nelineinoi Akustike* (Waves and Structures in Nonlinear Media without Dispersion. Applications to Nonlinear Acoustics) (Moscow: Fizmatlit, 2008)
18. Gurbatov S N, Saichev A I, Shandarin S F *Phys. Usp.* **55** 223 (2012); *Usp. Fiz. Nauk* **182** 233 (2012)
19. Ostrovsky L A, Gurbatov S N, Didenkulov I N *Acoust. Phys.* **51** 114 (2005); *Akust. Zh.* **51** 150 (2005);
20. Myasnikov L L *Zh. Tekh. Fiz.* **8** 1846 (1938)
21. Krassilnikov V A, Shklovskaya-Kordy V V, Zarembo L K *J. Acoust. Soc. Am.* **29** 642 (1957)
22. Zarembo L K, Krasil'nikov V A, Shklovskaya-Kordy V V *Dokl. Akad. Nauk SSSR* **109** 731 (1956)
23. Burov V A, Krasil'nikov V L *Dokl. Akad. Nauk SSSR* **118** 920 (1958)
24. Burov V A, Krasil'nikov V L *Dokl. Akad. Nauk SSSR* **124** 571 (1959)
25. Gorelik A G, Zverev V A *Akust. Zh.* **1** 339 (1955)
26. Zverev V A, Kalachev A I, Stepanov N S *Akust. Zh.* **13** 380 (1967)
27. Esipov I B, Zverev V A, Kalachev A I *Akust. Zh.* **22** 606 (1976)
28. Zverev V A *Akust. Zh.* **45** 685 (1999)
29. Eikhenval'd A A *Usp. Fiz. Nauk* **14** 552 (1934)
30. Efimov V B et al. *Fiz. Nizk. Temp.* **24** 116 (1998)
31. Khalatnikov I M *An Introduction to the Theory of Superfluidity* (New York: W.A. Benjamin, 1965); Translated from Russian: *Vvedenie v Teoriyu Sverkhtekuchesti* (Moscow: Nauka, 1965)
32. Lifshitz E M *Zh. Eksp. Teor. Fiz.* **14** 116 (1944)
33. Peshkov V P *Zh. Eksp. Teor. Fiz.* **16** 1000 (1946)
34. Peshkov V P *Zh. Eksp. Teor. Fiz.* **18** 857 (1948)
35. Brooks J S, Donnelly R J *J. Phys. Chem. Ref. Data* **6** 51 (1977)
36. Efimov V B et al. *JETP Lett.* **69** 767 (1999); *Pis'ma Zh. Eksp. Teor. Fiz.* **69** 716 (1999)
37. Maurer J, Tabeling P *Europhys. Lett.* **43** 29 (1998)
38. Stalp S R, Skrbek L, Donnelly R J *Phys. Rev. Lett.* **82** 4381 (1999)
39. Niemela J J, Sreenavasan K R, Donnelly R J *J. Low Temp. Phys.* **138** 537 (2005)
40. Charalambous D et al. *Phys. Rev. E* **74** 036307 (2006)
41. Krasil'nikov V A, Krylov V V *Vvedenie v Fizicheskuyu Akustiku* (Introduction into Physical Acoustics) (Moscow: Nauka, 1984)
42. Wilks J *The Properties of Liquid and Solid Helium* (Oxford: Clarendon Press, 1967)
43. Tyson J A, Douglass D H (Jr.) *Phys. Rev. Lett.* **21** 1308 (1968)
44. Khalatnikov I M *Teoriya Sverkhtekuchesti* (Theory of Superfluidity) (Moscow: Nauka, 1971)
45. Peshkov V P *Zh. Eksp. Teor. Fiz.* **19** 270 (1949)
46. Khalatnikov I M *Zh. Eksp. Teor. Fiz.* **23** 253 (1952)
47. Dessler A J, Fairbank W M *Phys. Rev.* **104** 6 (1956)
48. Zakharov V E, Sagdeev R Z *Dokl. Akad. Nauk SSSR* **192** 297 (1970)
49. Donnelly R J *Quantum Vortexes in Helium II* (Cambridge: Cambridge Univ. Press, 1991)
50. Nemirovskii S K, Tsoi A N *Cryogenics* **29** 985 (1989)
51. Makarov A et al. *Phys. Rev. B* **91** 094503 (2015)
52. Kitabatake S, Sawada Y *J. Phys. Soc. Jpn.* **45** 345 (1978)
53. Nemirovskii S K *Sov. Phys. Usp.* **33** 429 (1990); *Usp. Fiz. Nauk* **160** (6) 51 (1990)
54. Zinov'eva K N *Zh. Eksp. Teor. Fiz.* **25** (8) 235 (1953)
55. Hendry P C et al. *Nature* **368** 315 (1994)
56. Cummings J C, Schmidt D W, Wagner W J *Phys. Fluids* **21** 713 (1978)
57. Iznankin A Yu, Mezhov-Deglin L P *Sov. Phys. JETP* **57** 801 (1983); *Zh. Eksp. Teor. Fiz.* **84** 1378 (1983)
58. Lutset M O, Nemirovskii S K, Tsoi A N *Sov. Phys. JETP* **54** 127 (1981); *Zh. Eksp. Teor. Fiz.* **81** 249 (1981)
59. Turner T N *Phys. Fluids* **26** 3227 (1983)
60. Borisenko I Yu, Efimov V B, Mezhov-Deglin L P *Fiz. Nizk. Temp.* **14** 1123 (1988)
61. Dyumin N E, Svatko S V, Grigor'ev V N *Fiz. Nizk. Temp.* **15** (1) 89 (1989)
62. Smith M R et al. *Phys. Rev. Lett.* **71** 2583 (1993)
63. Chagovets T V, Skrbek L *Phys. Rev. Lett.* **100** 215302 (2008)
64. Vinen W F *Proc. R. Soc.* **242** 114 (1956)
65. Skrbek L, Gordeev A V, Soukup F *Phys. Rev. E* **67** 047302 (2003)
66. Morse P M *Vibration and Sound* 2nd ed. (New York: McGraw-Hill, 1948)
67. Zinov'eva K N *Sov. Phys. JETP* **4** 36 (1957); *Zh. Eksp. Teor. Fiz.* **31** 31 (1956)
68. Davidowitz H, L'vov Y, Steinberg V *Physica D* **84** 635 (1995)
69. Efimov V B et al. *J. Low Temp. Phys.* **156** (3–6) 95 (2009)
70. Betchov R *Phys. Fluids* **1** 205 (1958)
71. Chester W *J. Fluid Mech.* **18** 44 (1964)
72. Temkin S *Phys. Fluids* **11** 960 (1968)
73. Cruikshank D B (Jr.) *J. Acoust. Soc. Am.* **52** 1024 (1972)
74. Karabutov A A, Rudenko O V *Akust. Zh.* **25** 536 (1979)
75. Kaner V V, Rudenko O V, Khokhlov R V *Akust. Zh.* **23** 756 (1977)
76. Rudenko O V *JETP Lett.* **20** 203 (1974); *Pis'ma Zh. Eksp. Teor. Fiz.* **20** 445 (1974)
77. Karabutov A A, Lapshin E A, Rudenko O V *Sov. Phys. JETP* **44** 58 (1976); *Zh. Eksp. Teor. Fiz.* **71** 111 (1976)
78. Clauss G F *Appl. Ocean Res.* **24** 147 (2002)
79. Brazhnikov M Yu et al. *Fiz. Nizk. Temp.* **27** 1183 (2001)
80. Ezersky A et al. *Eur. J. Mech. B* **28** 521 (2009)
81. Lukaschuk S et al. *Phys. Rev. Lett.* **103** 044501 (2009)
82. Henry E, Alstrøm P, Levinsen M T *Europhys. Lett.* **52** 27 (2000)
83. Savelsberg R, van de Water W *Phys. Rev. Lett.* **100** 034501 (2008)
84. Falcon E, Fauve S, Laroche C *Phys. Rev. Lett.* **98** 154501 (2007)
85. Brazhnikov M Yu, Kolmakov G V, Levchenko A A *JETP* **95** 447 (2002); *Zh. Eksp. Teor. Fiz.* **122** 521 (2002)
86. Abdurakhimov L, Brazhnikov M, Levchenko A *Low Temp. Phys.* **35** 95 (2009); *Fiz. Nizk. Temp.* **35** 127 (2009)
87. Kolmakov G V et al. *Czech. J. Phys.* **46** (Suppl. 1) 83 (1996)
88. Efimov V B et al. *Low Temp. Phys.* **24** 81 (1998); *Fiz. Nizk. Temp.* **24** 116 (1998)
89. Efimov V B et al. *Low Temp. Phys.* **25** 407 (1999); *Fiz. Nizk. Temp.* **25** 551 (1999)
90. van Sciver S W *Cryogenics* **19** 385 (1979)
91. Brazhnikov M Yu et al. *Low Temp. Phys.* **30** 441 (2004); *Fiz. Nizk. Temp.* **30** 590 (2004)
92. Kolmakov G V et al. *Phys. Rev. Lett.* **97** 155301 (2006)
93. Falkovich G, Meyer M *Phys. Rev. E* **54** 4431 (1996)
94. Pokrovskii V L, Khalatnikov I M *Sov. Phys. JETP* **44** 1036 (1976); *Zh. Eksp. Teor. Fiz.* **71** 1974 (1976)
95. Landau L D, Lifshitz E M *Fluid Mechanics* (Oxford: Pergamon Press, 1987); Translated from Russian: *Gidrodinamika* (Moscow: Nauka, 1986)
96. Kolmakov G V *Low Temp. Phys.* **29** 495 (2003); *Fiz. Nizk. Temp.* **29** 667 (2003)
97. Kolmogorov A N *Proc. R. Soc. Lond. A* **434** 9 (1991); Translated from Russian: *Dokl. Akad. Nauk SSSR* **31** 299 (1941)
98. Kolmogorov A N *Dokl. Akad. Nauk SSSR* **31** 538 (1941)
99. Obukhov A M *Turbulentnost' i Dinamika Atmosfery* (Turbulence and Atmospheric Dynamics) (Leningrad: Gidrometeoizdat, 1988)
100. Zakharov V E, L'vov V S, Fal'kovich G *Kolmogorov Spectra of Turbulence* (Berlin: Springer-Verlag, 1992)
101. Kolmakov G V et al. *Phys. Rev. Lett.* **93** 074501 (2004)
102. Dyachenko A I, Korotkevich A O, Zakharov V E *Phys. Rev. Lett.* **92** 134501 (2004)
103. Kuznetsov E A *JETP Lett.* **80** 83 (2004); *Pis'ma Zh. Eksp. Teor. Fiz.* **80** 92 (2004)
104. Gurbatov S N *Akust. Zh.* **26** 551 (1980)
105. Zakharov V E, Filonenko N N *Zh. Prikl. Mech. Tekh. Fiz.* **8** (5) 62 (1967)
106. Haudin F et al. *Phys. Rev. E* **93** 043110 (2016)

107. Prokhorov A M (Ed.) *Fizicheskaya Entsiklopediya* (Encyclopedia of Physics) Vol. 5 (Moscow: Bol'shaya Rossiiskaya Entsiklopediya, 1998)
108. Rudenko O V *Sov. Phys. Acoust.* **29** 234 (1983); *Akust. Zh.* **29** 398 (1983)
109. Rudenko O V *Phys. Usp.* **38** 965 (1995); *Usp. Fiz. Nauk* **165** 1011 (1995)
110. Khovanov I A, Khovanova N A *Veroyatnostnye Metody Analiza Sluchainykh Dannykh* (Probabilistic Methods of Random Data Analysis) (Saratov: Izd. Saratovskogo Univ., Kolledzh, 2001)
111. Efimov V B, Ganshin A N, McClintock P V E *Phys. Rev. E* **78** 066611 (2008)
112. Ganshin A N et al. *New J. Phys.* **12** 083047 (2010)
113. Filatov S V et al. *JETP Lett.* **104** 702 (2016); *Pis'ma Zh. Eksp. Teor. Fiz.* **104** 714 (2016)
114. Phillips O M *J. Fluid Mech.* **107** 465 (1981)
115. Annenkov S Y, Shrira V I *Phys. Rev. Lett.* **96** 204501 (2006)
116. Chertkov M et al. *Phys. Rev. Lett.* **99** 084501 (2007)
117. Korotkevich A O *Phys. Rev. Lett.* **101** 074504 (2008)
118. Ganshin A N et al. *Phys. Rev. Lett.* **101** 065303 (2008)
119. Kuznetsov A P, Kuznetsov S P, Ryskin N M *Nelineinye Kolebaniya* (Nonlinear Oscillations) (Moscow: Fizmatlit, 2002)